Electronic Supplementary Information.

To Heat or not to Heat: a study of the performances of Iron Carbide Nanoparticles in Hyperthermia.

Juan Manuel Asensio,* Julien Marbaix, Nicolas Mille, Lise-Marie Lacroix, Katerina Soulantica, Pier-Francesco Fazzini, Julian Carrey, Bruno Chaudret*

Table of Content:

SI.1. Experimental Section

All syntheses of non-commercial compounds were performed under argon atmosphere either by using Schlenk techniques or in a glove box. Mesitylene, toluene and tetrahydrofurane (THF) were obtained from VWR Prolabo, then purified on alumina desiccant and degassed by bubbling Ar through the solution for 20 minutes. The commercial products, hexadecylamine (HDA, 99%) and palmitic acid (PA, 99%) were obtained from Sigma-Aldrich and used in the glove-box. The bis(amido)iron(II) dimer $\{Fe[N(SiMe_3)_2]_2\}_2$ was obtained from Nanomeps. All these compounds were used without any additional purification. NPs **Fe-ref** and **FeC-ref** were already prepared by Bordet et al.[1] in our previous communication.

The size and the morphology of the NPs were studied by transmission electronic microscopy (TEM). TEM grids were prepared by deposition of one drop of a colloidal solution containing the NPs on a copper grid covered with amorphous carbon. Conventional bright-field images were performed using JEOL microscopes (Model 1011 and 1400) working at 100 kV and 120 kV respectively. STEM and EDX analyses were performed using a Probe Corrected JEOL JEM-ARM200F Cold FEG equipped with a High Angle EDX detector working at 200 kV. XRD measurements were performed on a PANalytical Empyrean diffractometer using Co-Kα radiation (λ=0.1789 nm) at 45 kV and 40 mA. Magnetic measurements were performed on a Vibrating Sample Magnetometer (VSM, Quantum Device PPMS Evercool II). Thermogravimetric analyses (TGA) were performed in a TGA/DSC 1 STAR System equipped with an ultra-microbalance UMX5, a gas switch GC200 and sensors DTA and DSC. DLS were measured with a Nanotrac Ultra instrument. XRD and VSM studies were carried out on compact powder samples that were prepared and sealed under argon atmosphere. To disperse some of the samples in tetracosane, the NPs were mixed with the matrix in a THF solution and sonicated for 30 minutes at 60 ºC. Slow evaporation of the solvent under sonication resulted in pale-grey powders that were prepared for VSM analyses as above indicated. The iron state and its environment were analysed by Mössbauer spectroscopy (WISSEL, ^{57}Co source). SAR measurements were performed by calorimetry experiments following the protocol already described in our previous work,[1] using a coil with a fixed frequency of 93 kHz (see below for more details).

SI.1.1. Synthesis of Fe(0) nanoparticles

In a typical synthesis, the Fe(0) NPs were prepared as following: in the glove box, 2.62 mmol of PA (666.4 mg) dissolved in 20 mL of degassed mesitylene were added to a green solution of 1.00 mmol of $\{Fe[N(SiMe_3)_2]_2\}_2$ (753.2 mg) in 10 mL of mesitylene in a Fischer Porter bottle. The solution turned from green to yellow. Then, 2.00 mmol of HDA (483.0 mg) solved in 10 mL of mesitylene were added. The bottle was pressurized with H_2 (2 bar) and placed in an oil bath at 150°C for 72 h under vigorous magnetic stirring (400 rpm). The reaction was stopped, and the NPs were recovered by decantation assisted by a magnet. The

mixture was introduced into the glove box and washed 3 times (3×10 mL) with toluene and 3 times (3×20 mL) with THF. Then, NPs **Fe-1** were dried under vacuum. TGA analysis showed that the black powder obtained contained ~75 wt% of iron. (Mass of powder obtained: 100-120 mg) The NPs were further characterized by XRD, VSM and TEM.

SI.1.2. Synthesis of iron carbide nanoparticles FeC-1 and FeC-2.

FeC NPs were obtained through the carbidization of preformed Fe(0) NPs. NPs **Fe-1** (50 mg, ~0.67 mmol of iron) were dispersed in mesitylene (10 mL), and the mixture was pressurized with CO/H_2 (2 bar / 2 bar) in a Fischer Porter bottle. The solution was heated at 150°C for 96 hours to obtain NPs **FeC-1** or for 2 days to obtain NPs **FeC-2**. At the end of the reaction, the NPs were recovered by decantation assisted by a magnet and were washed 3 times with toluene (3×10 mL). The NPs were then dried under vacuum to give a black powder. (Mass of powder obtained: ~40 mg).TGA analysis showed a 73 wt% of Fe in NPs **FeC-1** and a 75 wt% of Fe in NPs **FeC-2**. The NPs were further characterized by XRD, VSM and TEM and the SAR was determined for the NPs **FeC-2**.

SI.1.3. Synthesis of iron carbide nanoparticles FeC-3.

NPs **FeC-1** (50 mg, ~0.67mmol of iron) and 30 mg of palmitic acid (PA) were dispersed in mesitylene (10 mL) in a Fischer Porter bottle. The solution was heated at 150°C for 2 hours. Then, the NPs were recovered by decantation assisted by a magnet and were washed 3 times with toluene (3×10 mL). The NPs were further dried under vacuum. (Mass of powder obtained: ~35 mg). TGA analysis showed that the black powder obtained contained a 70 wt% of iron. The NPs were further characterized by XRD, VSM and TEM.

SI.1.4. Synthesis of iron carbide nanoparticles FeC-4 to FeC-9.

NPs **Fe-1** (50 mg, ~0.67mmol of iron) were dispersed in mesitylene (10 mL). A 1:1 mixture in mass of PA/HDA, 20, 30, 50 or 100 mg for NPs **FeC-4, FeC-5, FeC-6** and **FeC-7** respectively, or 50 mg of PA or HDA, for NPs **FeC-8** and **FeC-9** respectively, was added. Then, the same method above described for the preparation of NPs **FeC-1** and **FeC-2** was followed. (Mass of powder obtained: ~40 mg). TGA analysis showed that the black powder obtained contained ~70 wt% of iron. The NPs were further characterized by XRD, TEM and their SAR was determined. All the syntheses were scalable when keeping constant all the ratios between the reagents and the solvent.

SI.2. Hyperthermia measurements

For a typical hyperthermia experiment, an air-tight tube containing about 10 mg of iron carbide or iron/iron carbide nanocrystals dispersed in 0.5 mL of mesitylene was filled under inert atmosphere. The tube was then placed in a calorimeter containing 2.5 mL of deionized water, the temperature of which was monitored during the experiment. The calorimeter was exposed to an alternative magnetic field for a time varying between 10 and 40 s so that the temperature rise never exceeded 20°C. The temperature rise at the end of the magnetic field application was always measured after shaking the calorimeter to ensure the temperature homogeneity, which was measured by two probes (at the top and the bottom of the calorimeter). The temperature rise was determined after this process from the mean slope of the ΔT/Δt function. Then the raw SAR values were calculated using the expression:

$$SAR = \frac{\sum_i C_{pi} m_i}{m_{Fe}} \times \frac{\Delta T}{\Delta t}$$

where Cp_i and m_i are the specific heat capacity and the mass for each component respectively (Cp = 449 $J.kg^{-1}.K^{-1}$ for Fe NPs, Cp = 1750 $J.kg^{-1}.K^{-1}$for mesitylene, Cp = 4186 $J.kg^{-1}.K^{-1}$ for water and Cp = 720 $J.kg^{-1}.K^{-1}$ for glass), and m_{Fe} is the mass of pure iron in $Fe_{2.2}C$ NPs determined by Thermogravimetric Analysis.

The raw SAR values were corrected from the calorimeter losses, which were previously calibrated. For the calibration, a sample containing nanoparticles displaying moderate SAR was exposed for different time periods to an alternating magnetic field of 47 mT, 100 kHz. For each time, the SAR of the sample was measured. The SAR measured for an exposure time of 5s is considered as the “real” SAR (no losses). For longer exposure times, the difference between the measured SAR and the “real” SAR allows the determination of a corrective factor. The calibration curve is displayed below.

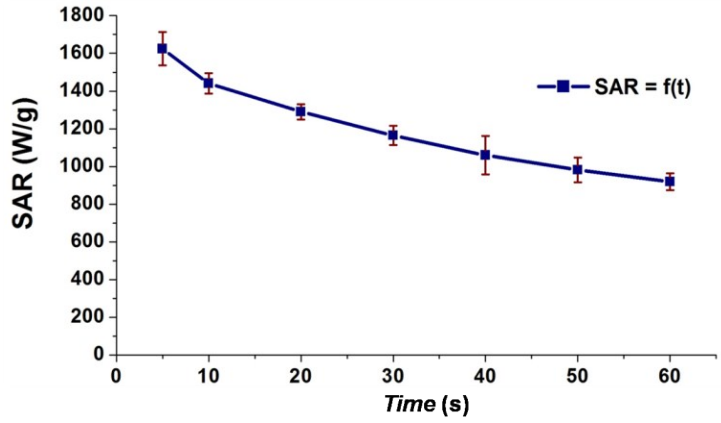

Exposure time (s)	Average SAR (W/g)	Corrective factor
5	1624	1,0
10	1440	1,11
20	1290	1,21
30	1165	1,28
40	1060	1,35
50	981	1,40
60	919	1,43

For the samples presented in this article, the measurement times were often comprised between 10 and 20s.

SI.3. Characterization of the agglomerated sample FeC-1

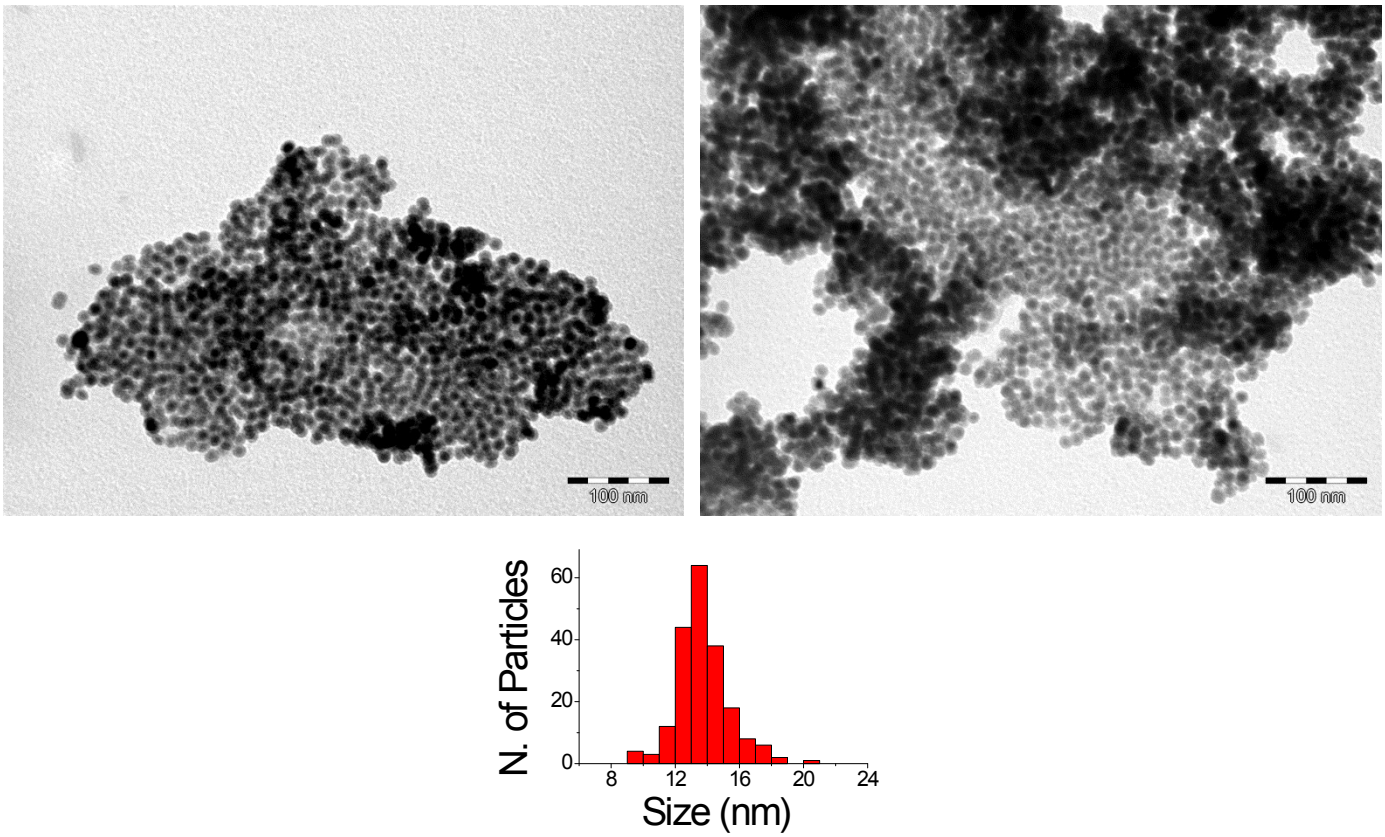

Figure S1. TEM images and size distribution of agglomerated NPs **FeC-1**.

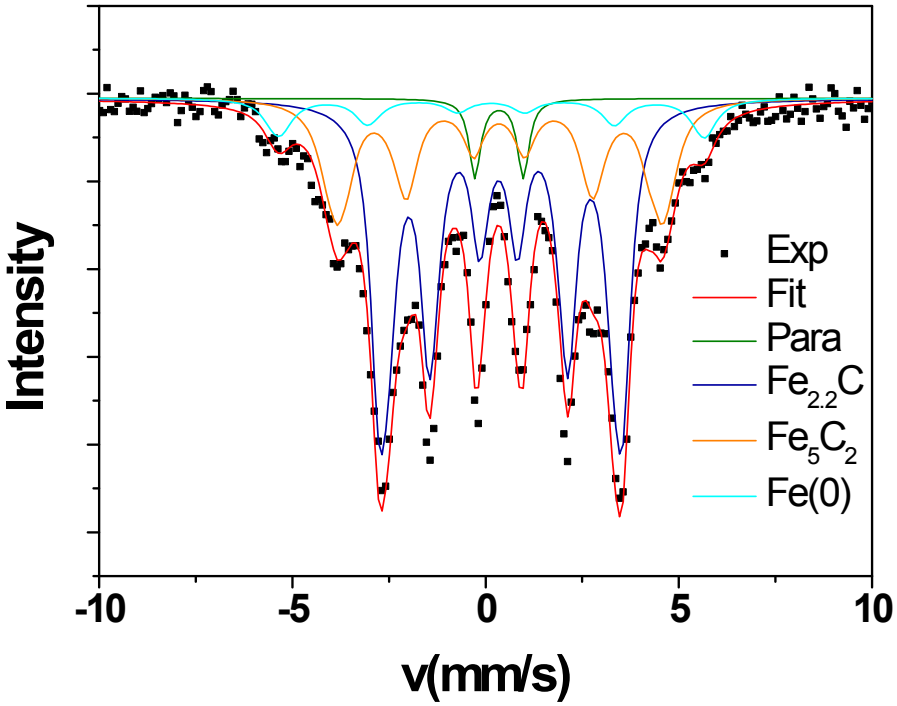

Phases	δ (mm/s)	Q (mm/s)	$\mu_0 H_{hyp}$ (T)	W (mm/s)	%	
Paramgnetic species	0.35	1.25		0.18	4	4
$Fe_{2.2}C$	0.37	0.03	18.1	0.3	26.8	59.6
	0.36	0.03	19.6	0.25	32.8	
Fe_5C_2	0.34		27	0.4	16.9	28.1
	0.33		24.3	0.3	7.5	
	0.37		25.9	0.2	3.7	
Fe(0)	0.08		35	0.25	0.5	8.3
	0.15		34	0.4	7.8	

Figure S2. Low temperature (4 K) Mössbauer study of iron carbide nanoparticles **FeC-1**. (a) Mössbauer spectrum, (b) fitting parameters and resulting nanoparticles composition.

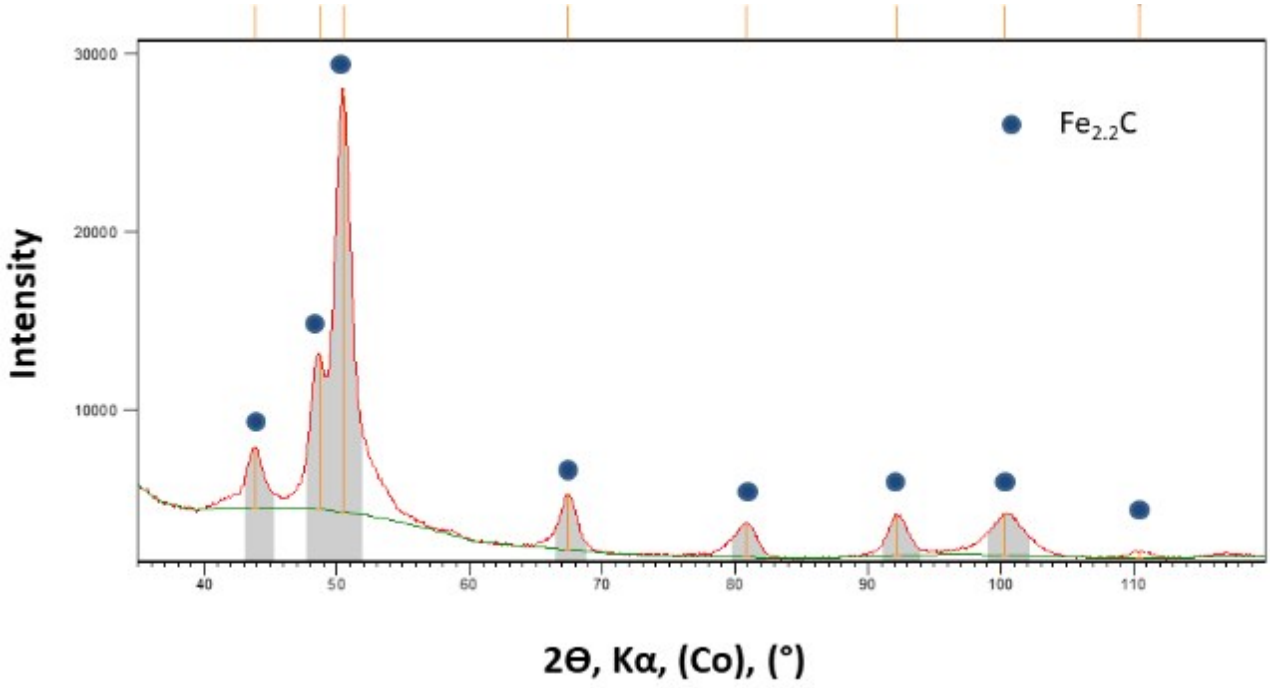

Figure S3. XRD diffractogram of the agglomerated NPs **FeC-1**. The labelled peaks correspond to the $Fe_{2.2}C$ phase.

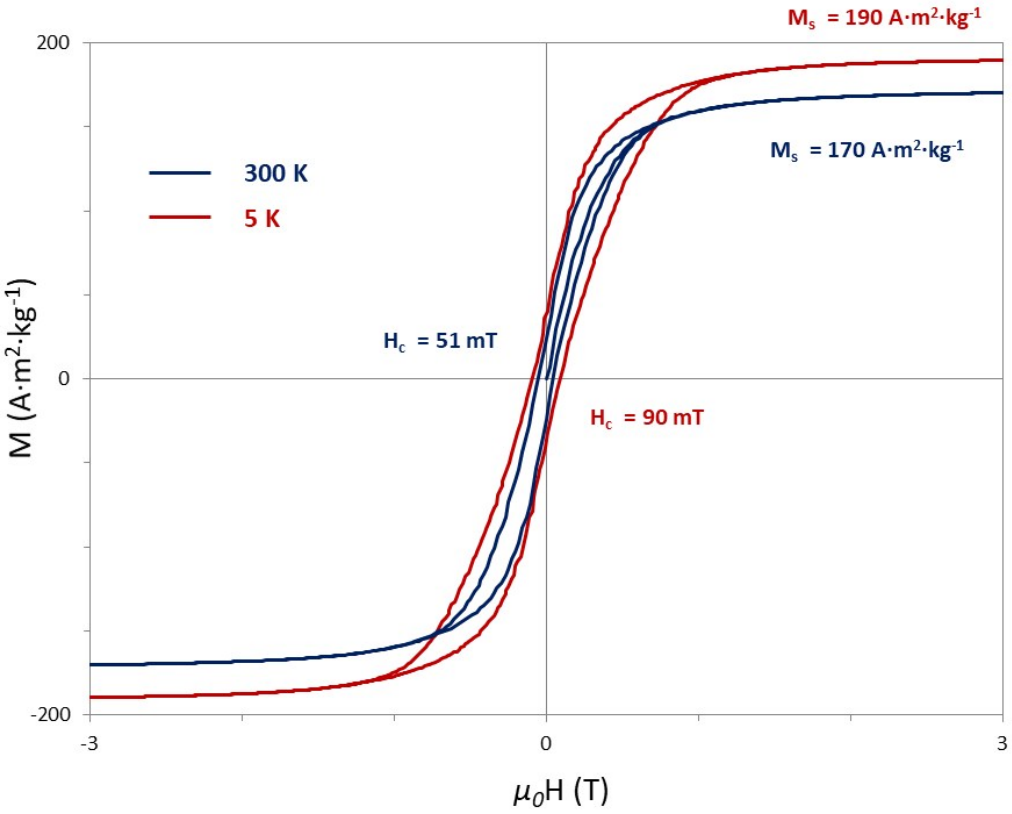

Figure S4. Hysteresis loops measured by VSM analysis for NPs **FeC-1** at 300 K and 5 K.

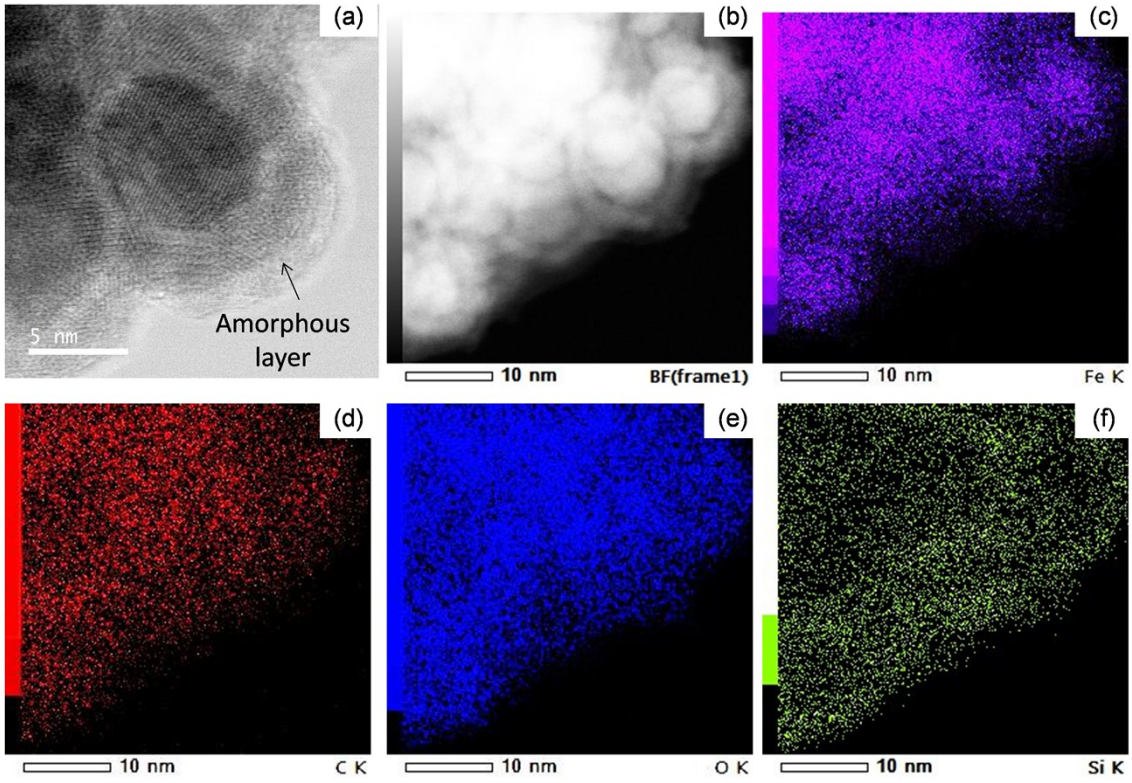

Figure S5. (a) HRTEM-BF (Bright field) picture of a nanoparticle of the non-heating agglomerated **FeC-1** NPs showing the SiO_2 amorphous embedding layer, (b) STEM-HAADF image of one agglomerate and (c-f) EDX mapping of **FeC-1** NPs showing the elements (c) Fe, (d) C, (e) O and (f) Si.

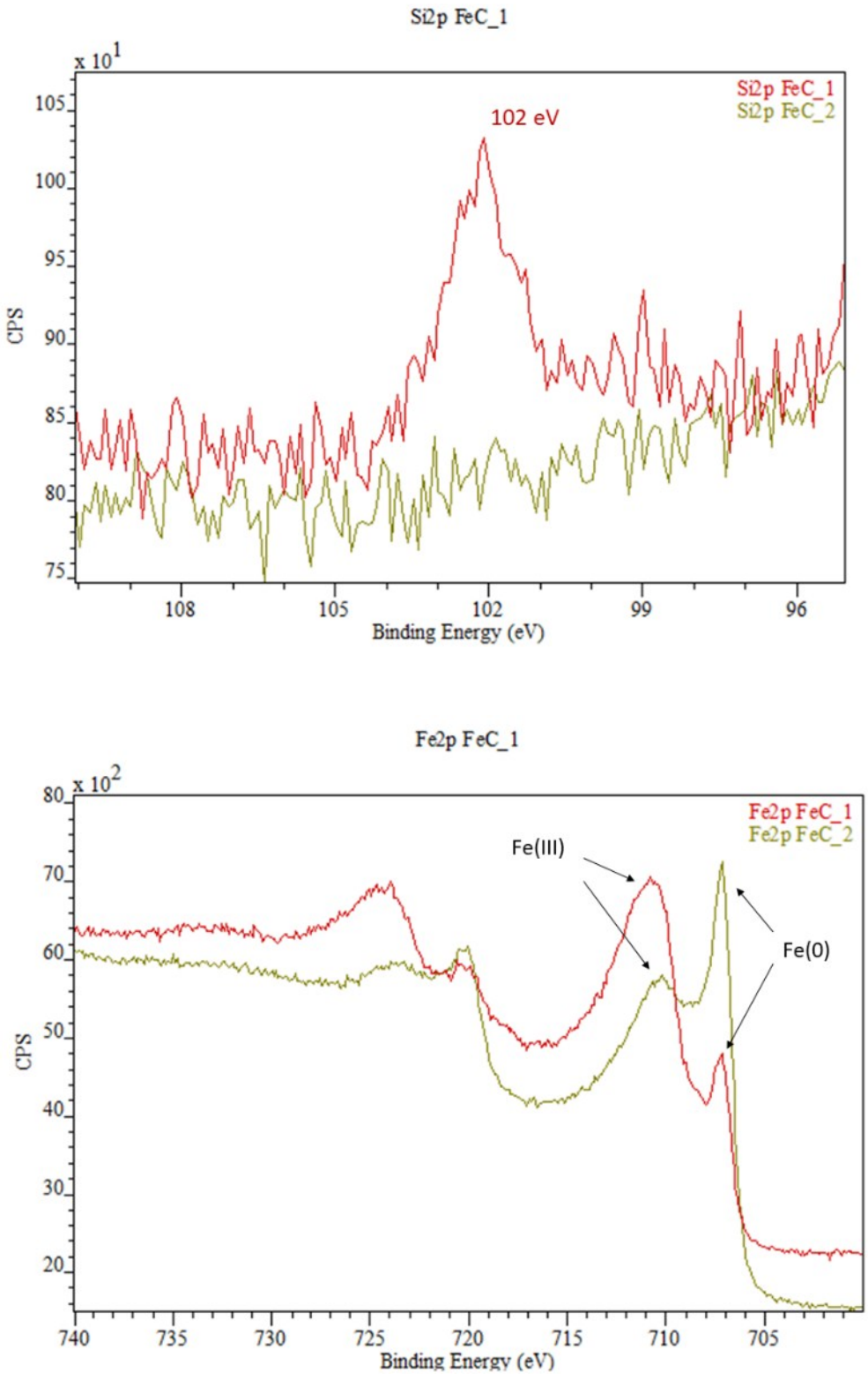

Fig S6. XPS spectra of NPs **FeC-1** (red) and **FeC-2** (green) for the $2p_{3/2}$ orbital of Si (up) and Fe(down).

SI.4. Characterization of the NPs FeC-2

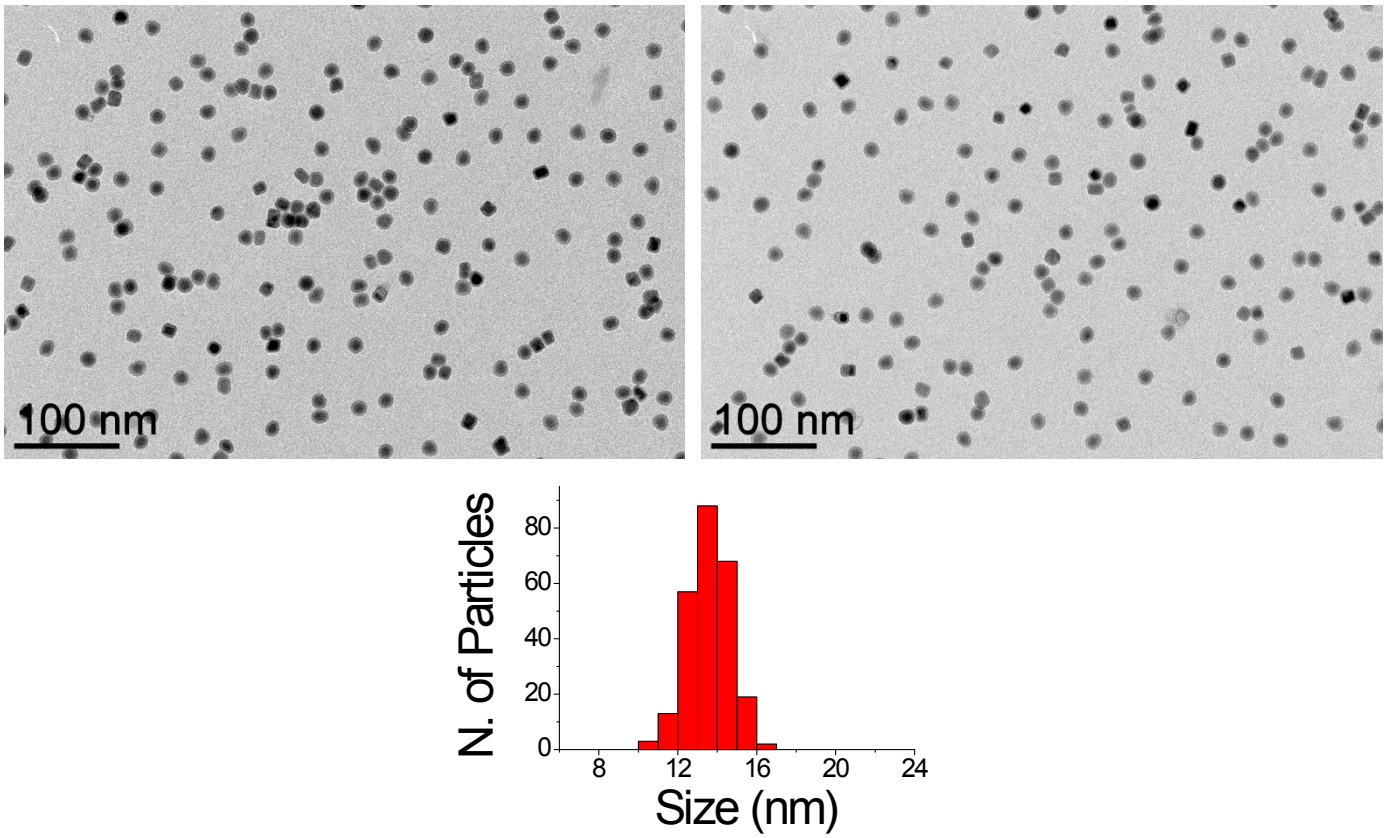

Figure S7. TEM images and size distribution of NPs **FeC-2**.

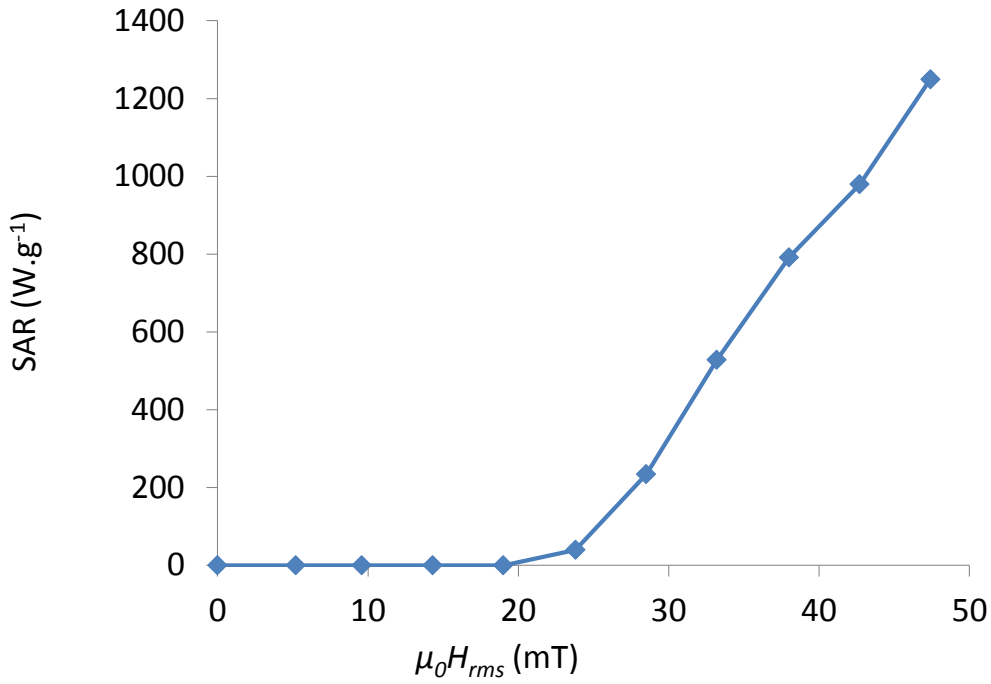

Fig S8. Heating power measurement at 93 kHz for NPs **FeC-2**.

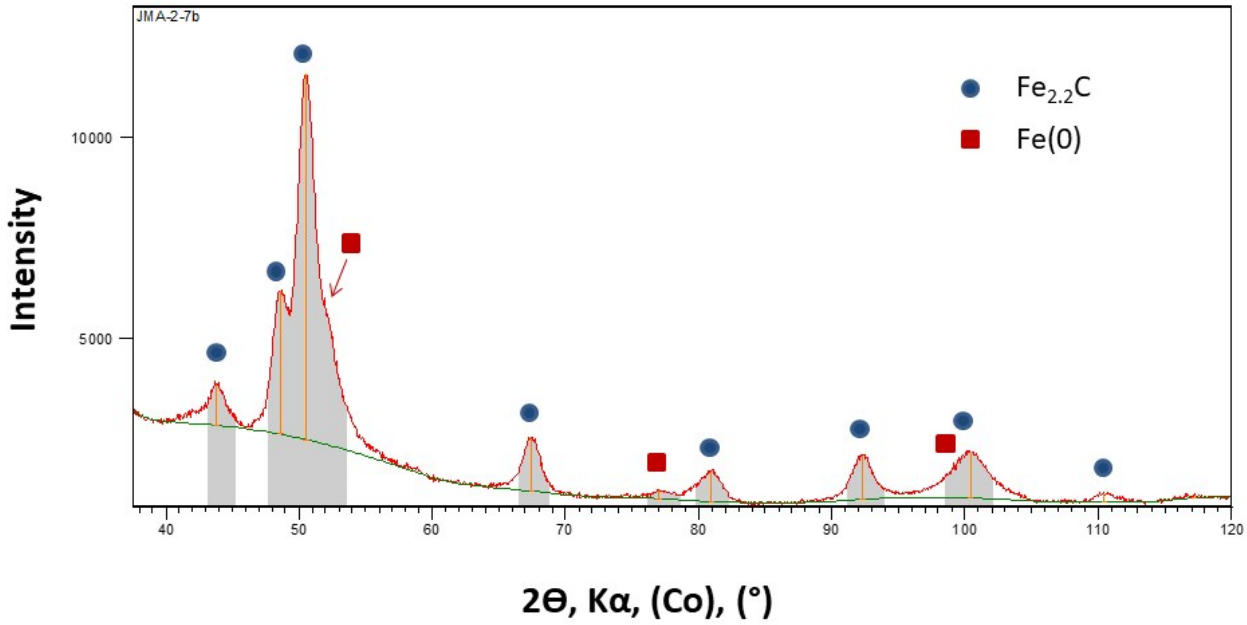

Figure S9. XRD diffractogram of NPs **FeC-2**. The peaks labelled in blue correspond to the $Fe_{2.2}C$ phase and the peaks labelled in red correspond to the Fe(0) phase.

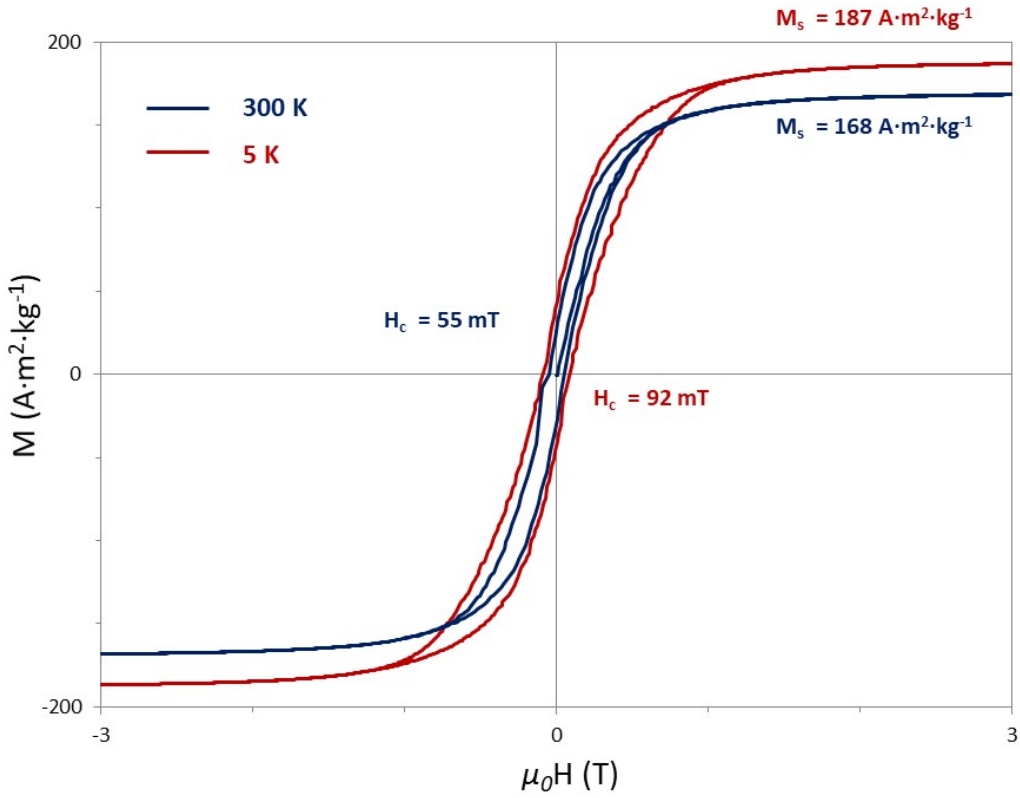

Figure S10. Hysteresis loops measured by VSM analysis for NPs **FeC-2** at 300 K and 5 K

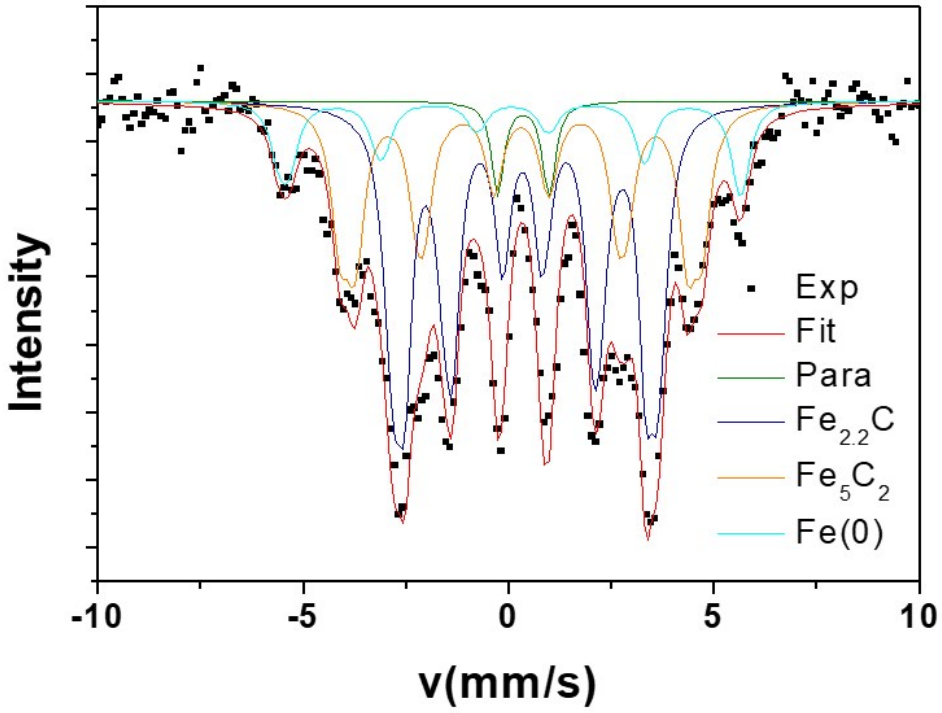

Phases	δ (mm/s)	Q (mm/s)	μ_0H_{hyp} (T)	W (mm/s)	%	
Paramagnetic species	0.35	1.25		0.18	4	4
$Fe_{2.2}C$	0.36	0.03	18.1	0.2	20	51.8
	0.37	0.03	19.8	0.25	25.6	
	0.35	0.03	20.7	0.25	6.2	
Fe_5C_2	0.3		25.1	0.25	17	32
	0.3		27.3	0.25	15	
Fe(0)	0		34.5	0.25	6.6	12.2
	0.18		34.2	0.25	5.6	

Figure S11. Low temperature (4 K) Mössbauer study of iron carbide nanoparticles **FeC-2**. (a) Mössbauer spectrum, (b) fitting parameters and resulting nanoparticles composition.

SI.5. Characterization of the NPs FeC-3

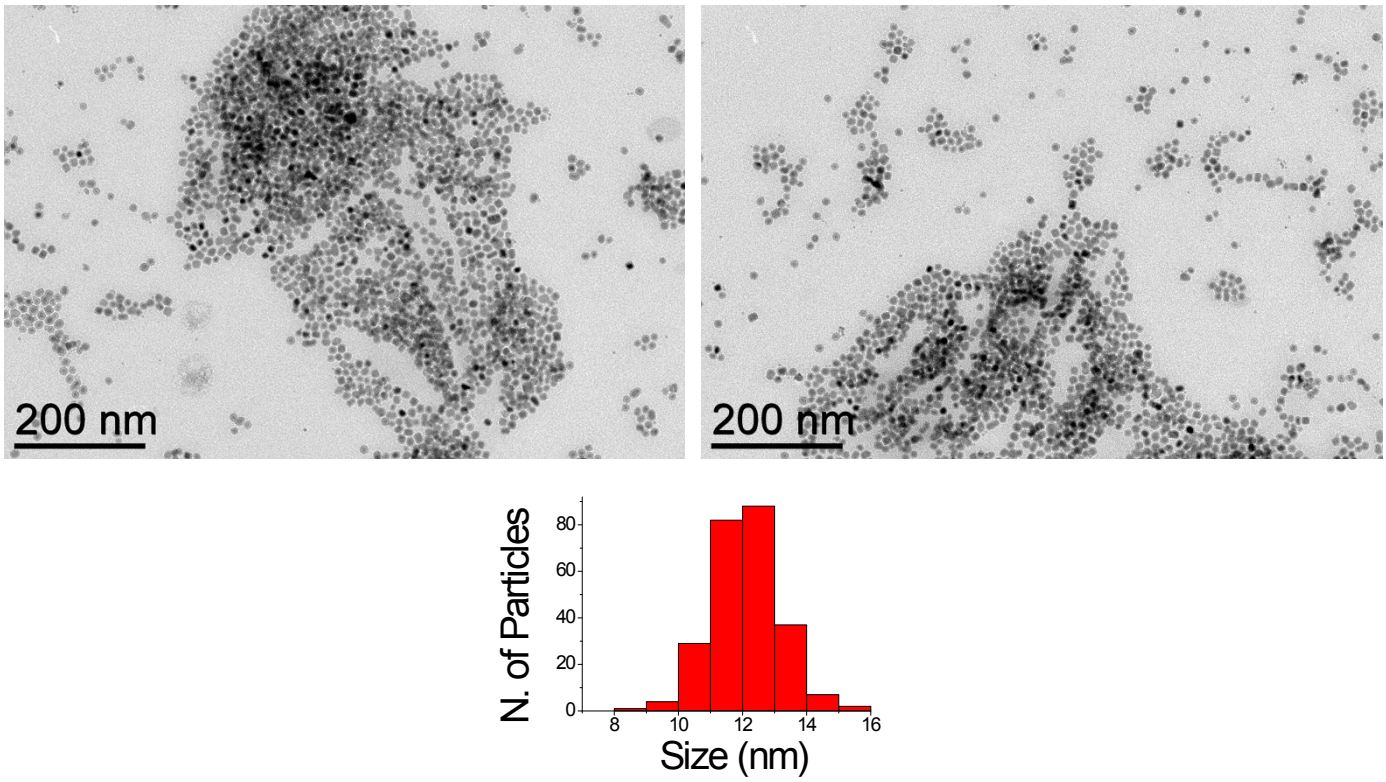

Figure S12. TEM images and size distribution of NPs **FeC-3** obtained after re-dispersion of NPs **FeC-1**. The images were taken at different regions of the TEM grid to show the different degree of agglomeration.

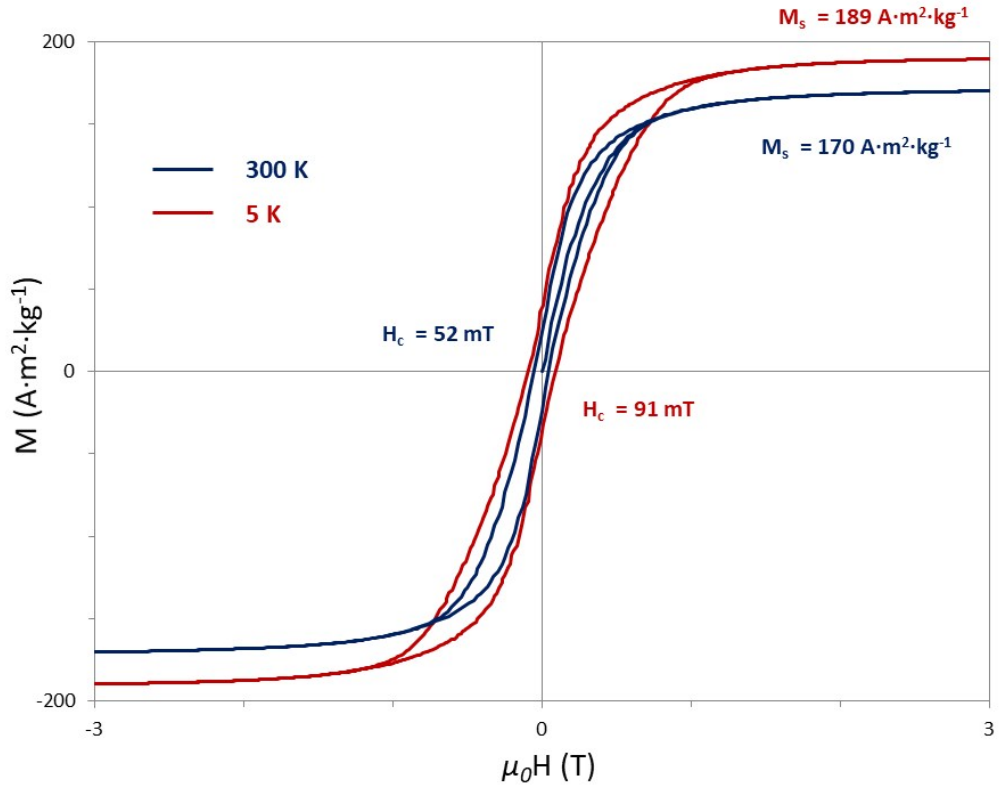

Figure S13. Hysteresis loops measured by VSM analysis for NPs **FeC-3** at 300 K and 5 K

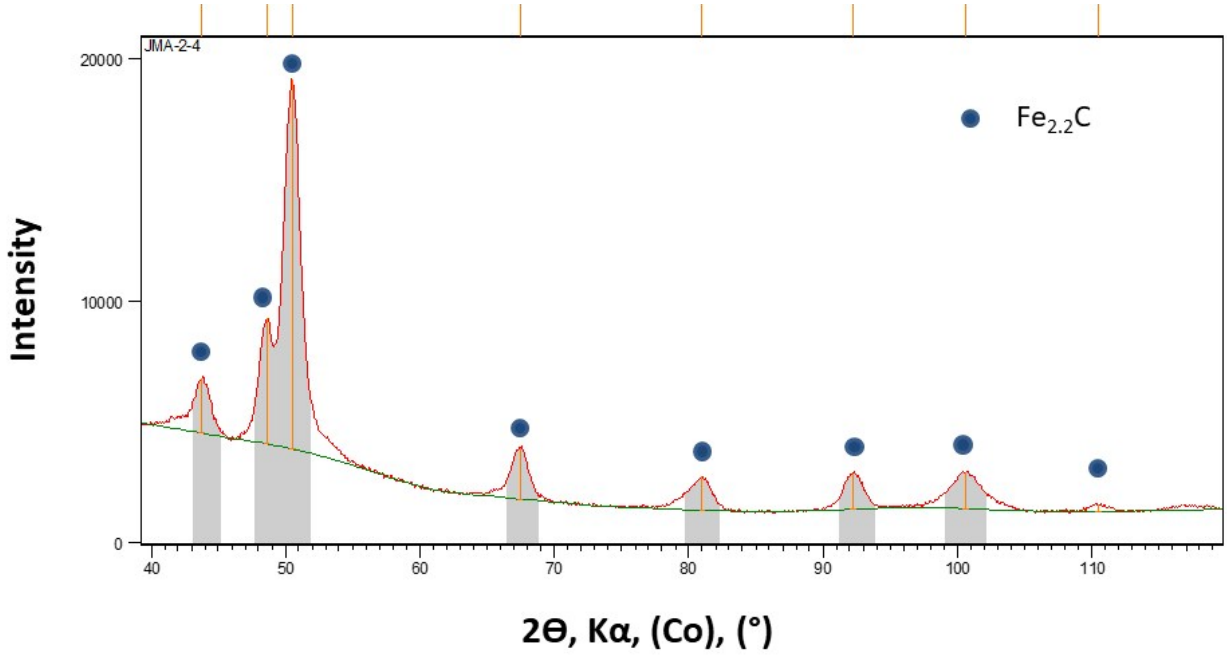

Figure S14. XRD diffractogram of NPs **FeC-3**. The labelled peaks correspond to the $Fe_{2.2}C$ phase.

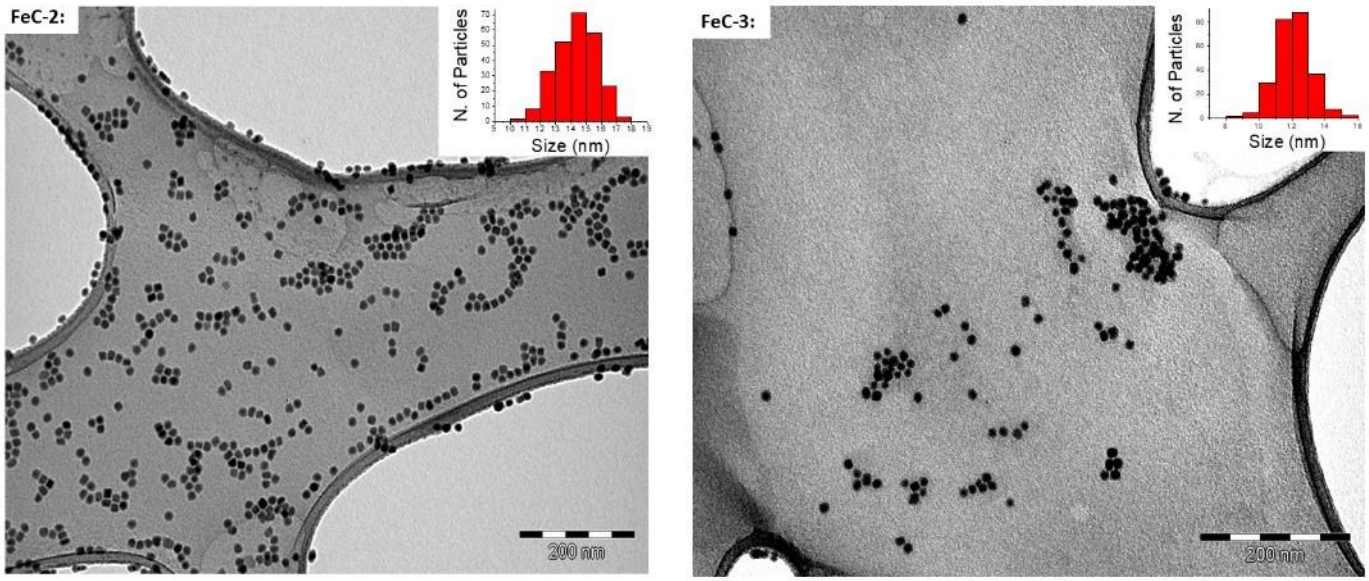

Figure S15. Representative TEM images and size distributions of NPs **FeC-2** and **FeC-3** in the hollow copper grids. The pictures show the different degree of dispersion of the FeC NPs thorough the TEM grids, which agrees with the presence of stronger interactions in the case of NPs **FeC-3**.

SI.6. Comparison between the NPs FeC-2 and FeC-3

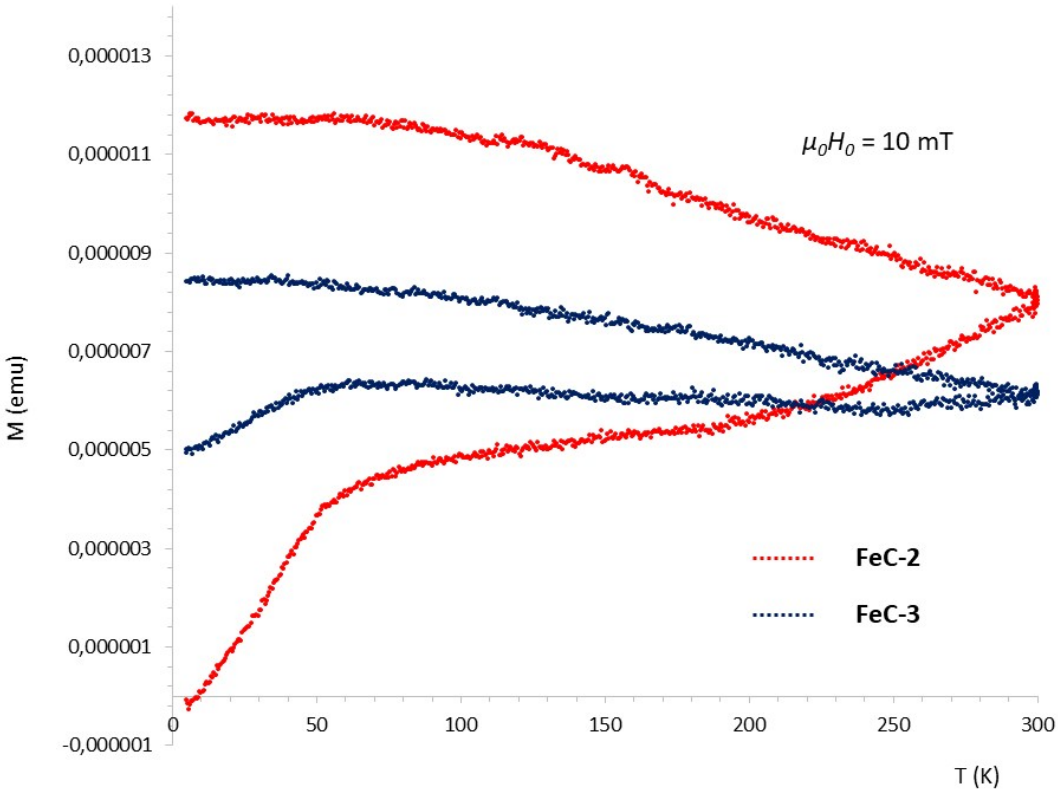

Figure S16. Zero-field cooled – field cooled experiments (ZFC/FC) for NPs **FeC-2** and **FeC-3** at $\mu_0 H_0$ of 10 mT. The graph shows the variation of the M vs. T.

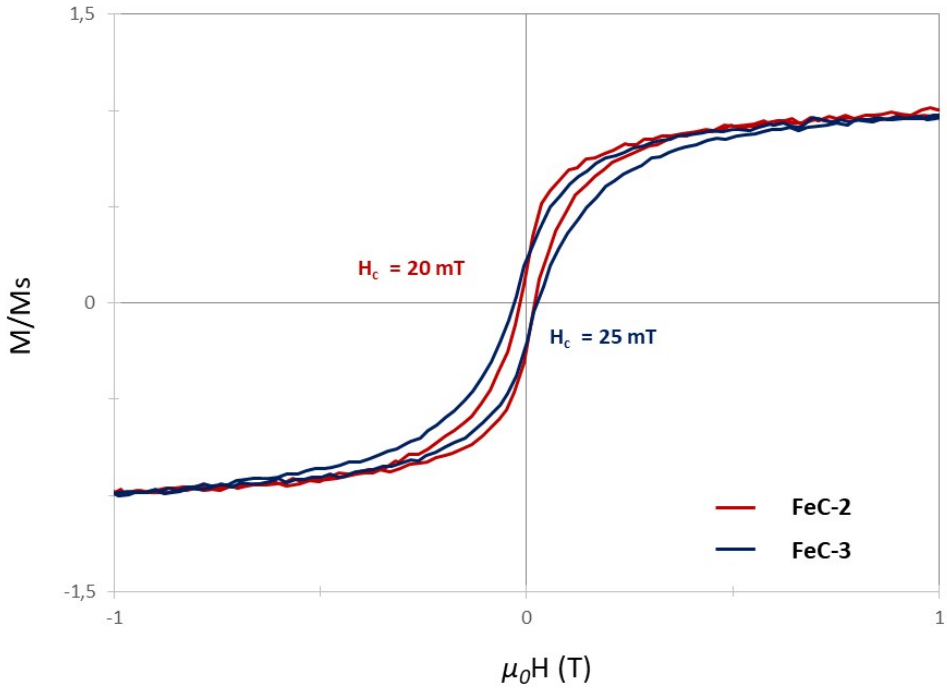

Figure S17. Hysteresis loops measured by VSM for NPs **FeC-2** (red) and **FeC-3** (blue) at 300 K after dilution in tetracosane. The graphs have been mathematically treated to remove the diamagnetic response of the tetracosane. The magnetization is normalized respect to the Ms value

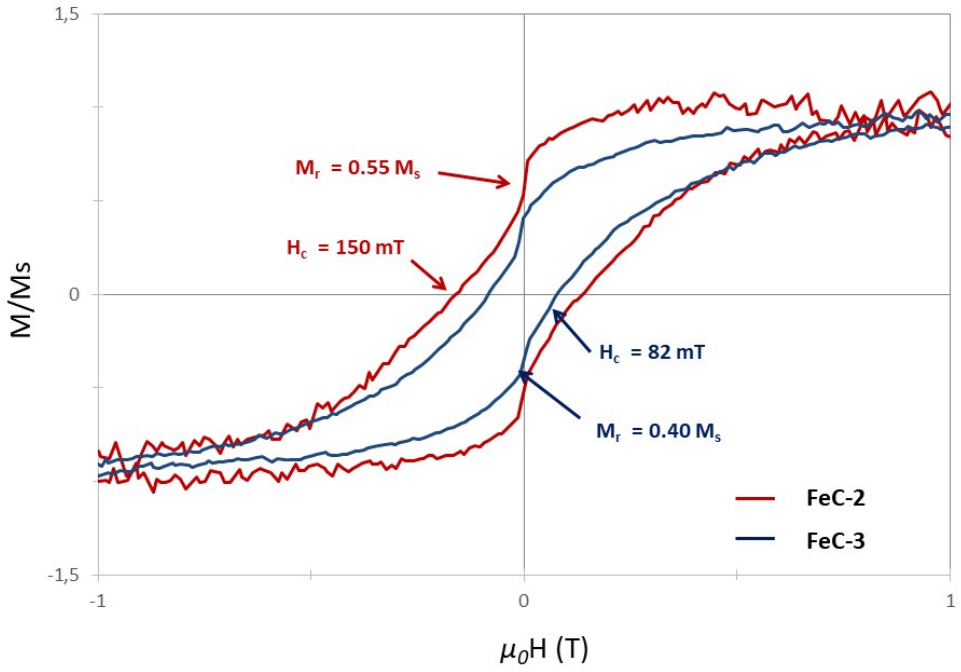

Figure S18. Hysteresis loops measured by VSM for NPs **FeC-2** (red) and **FeC-3** (blue) at 5 K after dilution in tetracosane. The graphs have been mathematically treated to remove the diamagnetic response of the tetracosane. The magnetization is normalized respect to the Ms value.

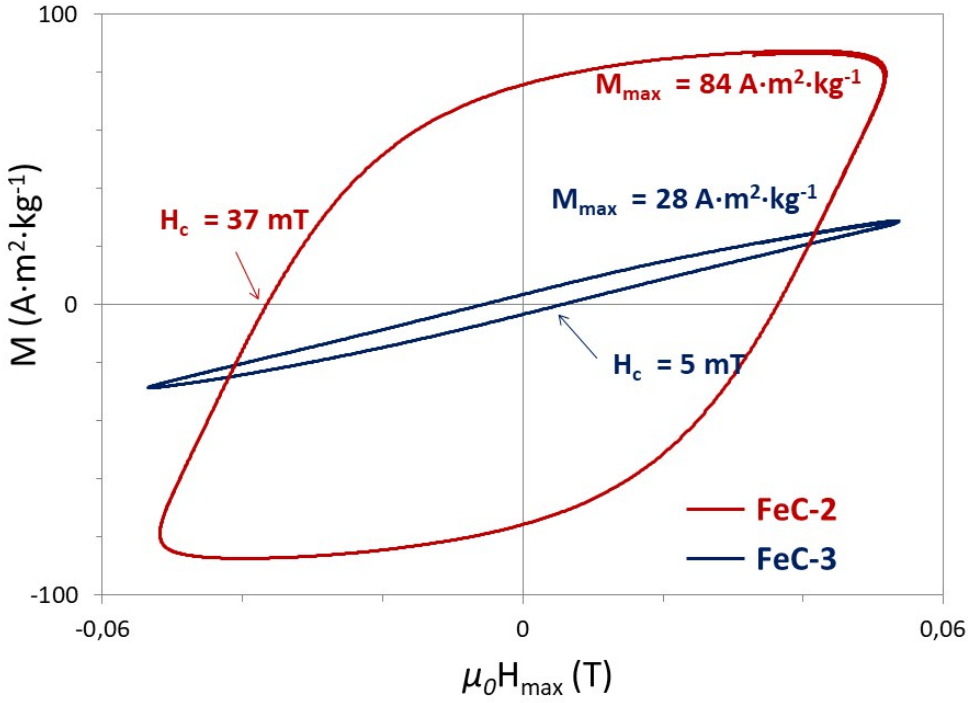

Figure S19. High-frequency hysteresis cycles for NPs **FeC-2** (red) and **FeC-3** (blue), when applying an alternating magnetic field of $\mu_0 H_{rms}$ of 37 mT with a f of 50 kHz.

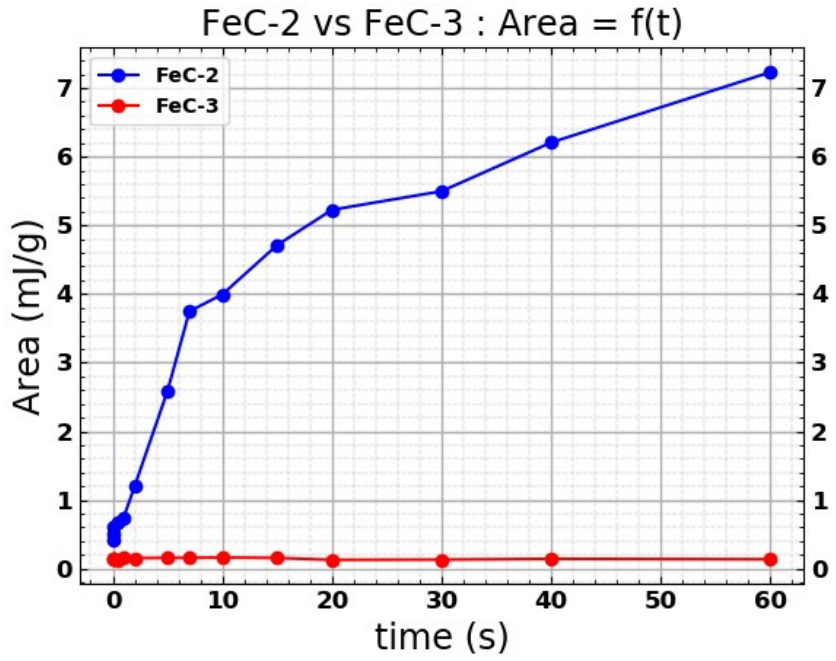

Figure S20. Evolution of the area of the hysteresis cycles as a function of time for NPs **FeC-2** (blue) and **FeC-3** (red), when applying an alternating magnetic field of $\mu_0 H_{rms}$ of 33 mT with a *f* of 50 kHz.

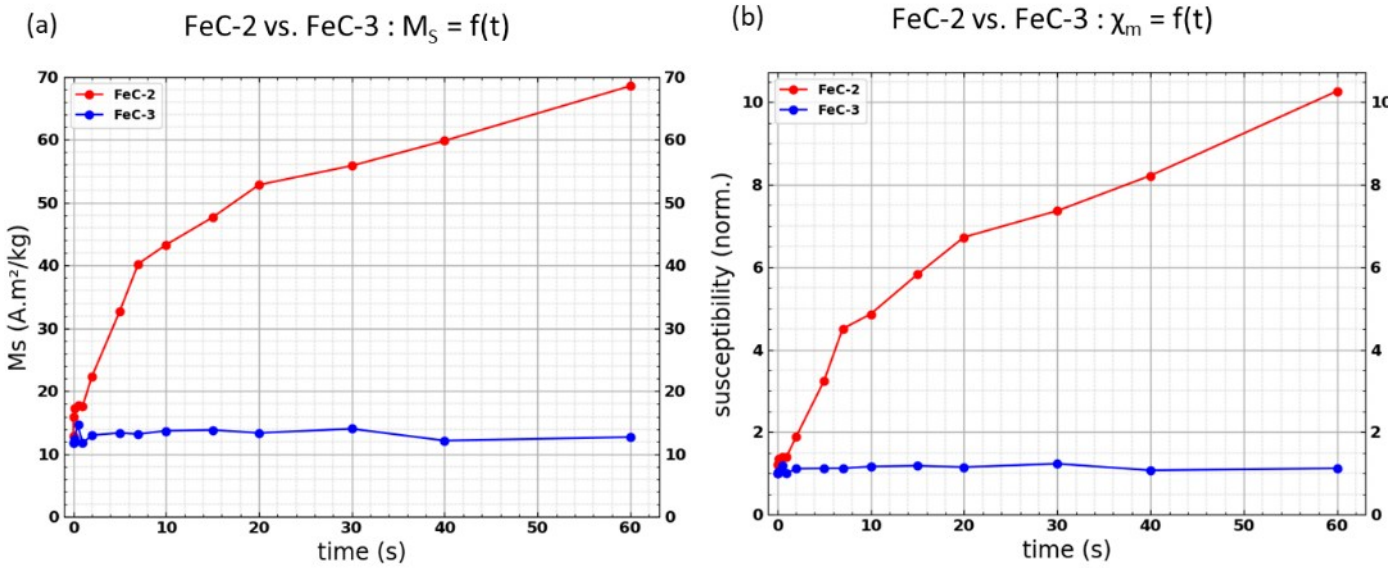

Figure S21. Evolution of (a) saturation magnetization and (b) normalized magnetic susceptibility as a function of time for NPs **FeC-2** (red) and **FeC-3** (blue), after application of an alternating magnetic field of $\mu_0 H_{rms}$ of 33 mT with a *f* of 50 kHz.

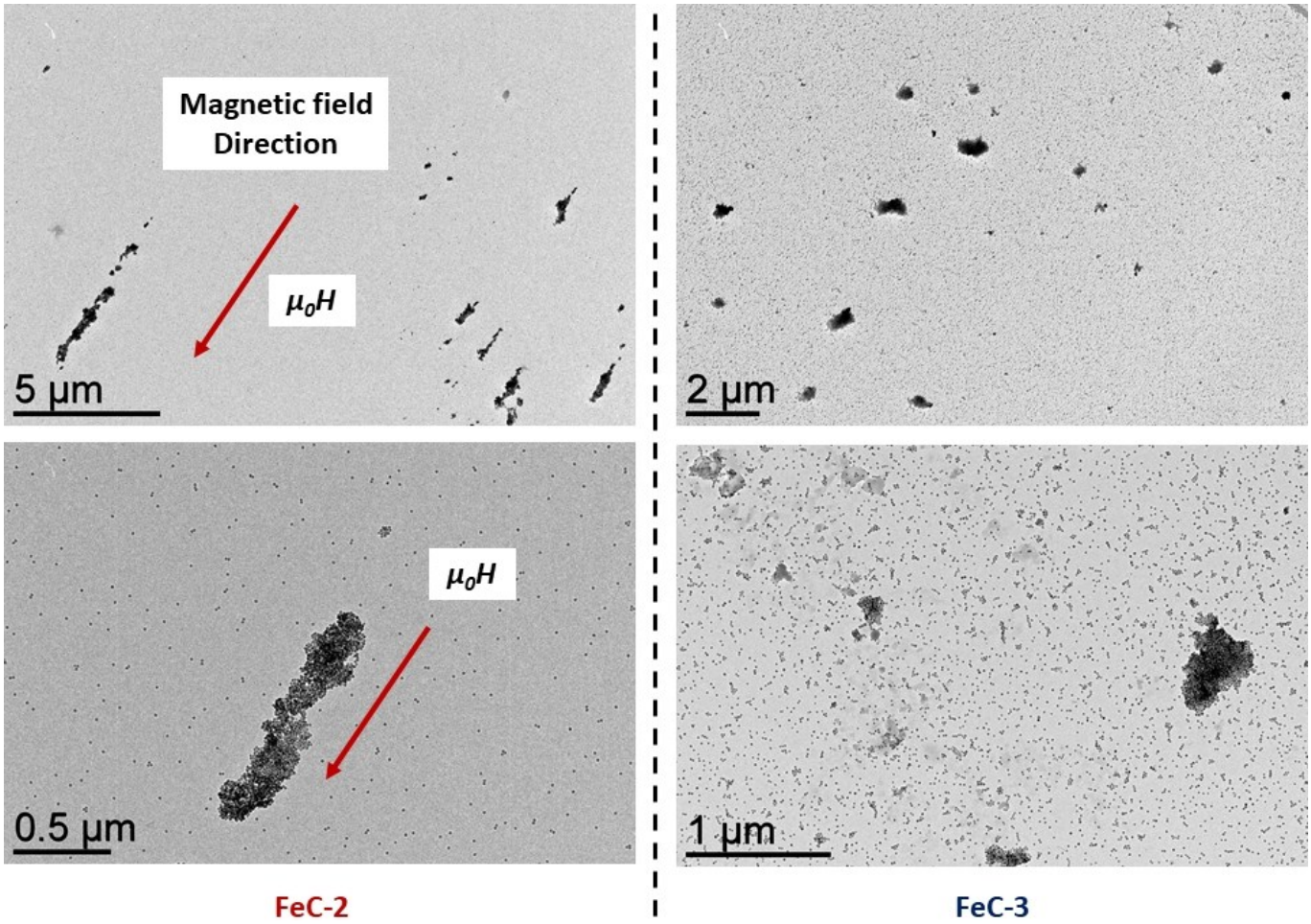

Figure S22. TEM images of the NPs **FeC-2** (left) and **FeC-3** (right) when one drop of the hyperthermia solution was deposed on the grid in presence of a magnetic field of $\mu_0 H_{rms}$ of 47 mT with a *f* of 93 kHz.

SI.7. Characterization of NPs FeC-4 to FeC-7.

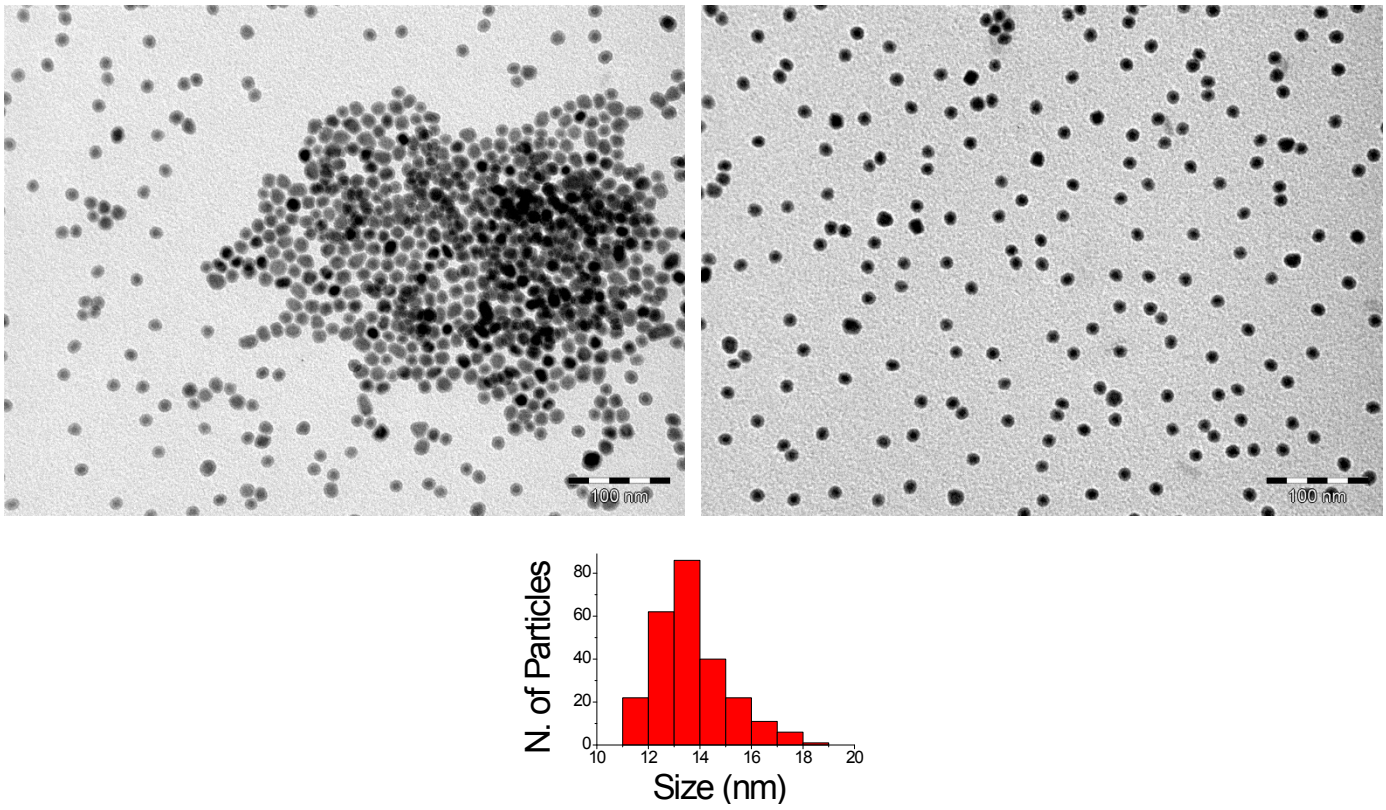

Figure S23. TEM images and size distribution of NPs **FeC-4** obtained after addition of 20 mg of a 1:1 mixture of PA and HDA.

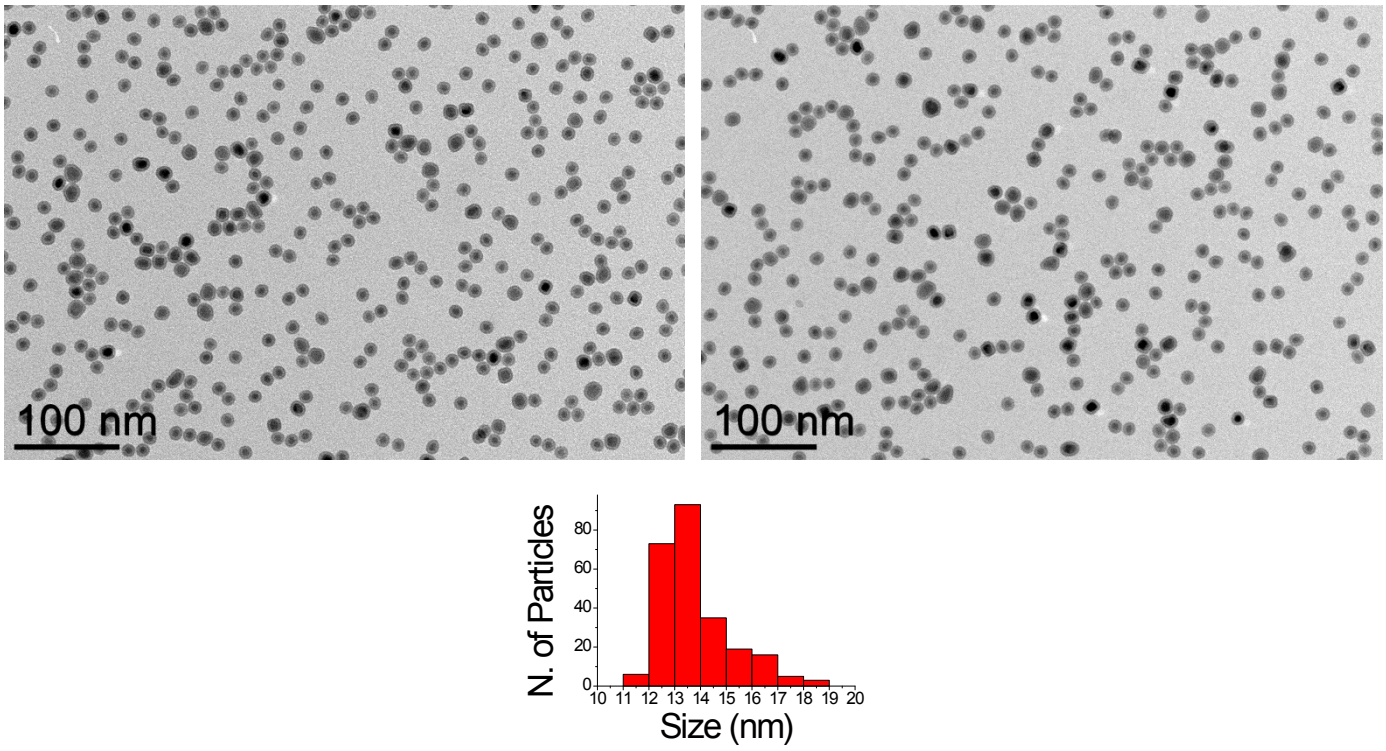

Figure S24. TEM images and size distribution of NPs **FeC-5** obtained after addition of 30 mg of a 1:1 mixture of PA and HDA.

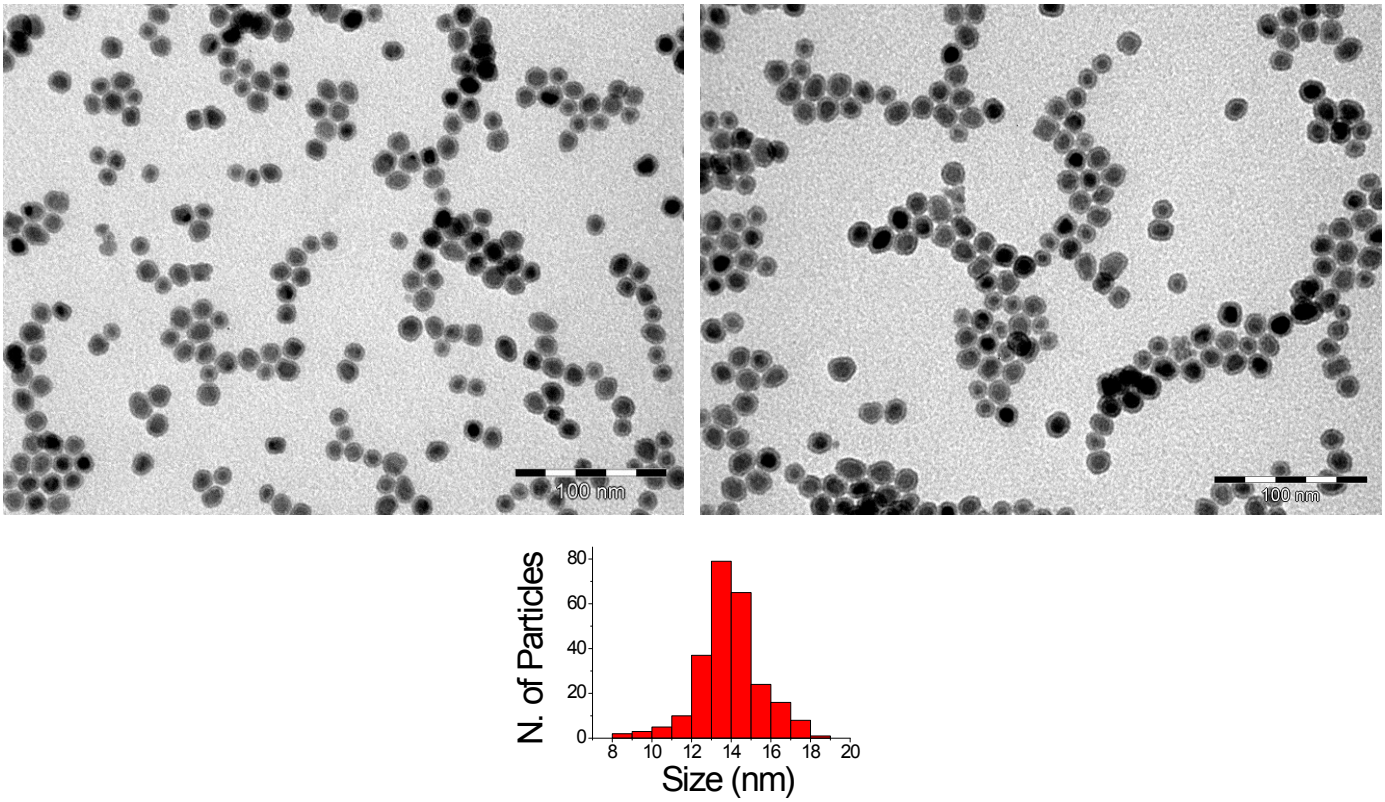

Figure S25. TEM images and size distribution of NPs **FeC-6** obtained after addition of 50 mg of a 1:1 mixture of PA and HDA.

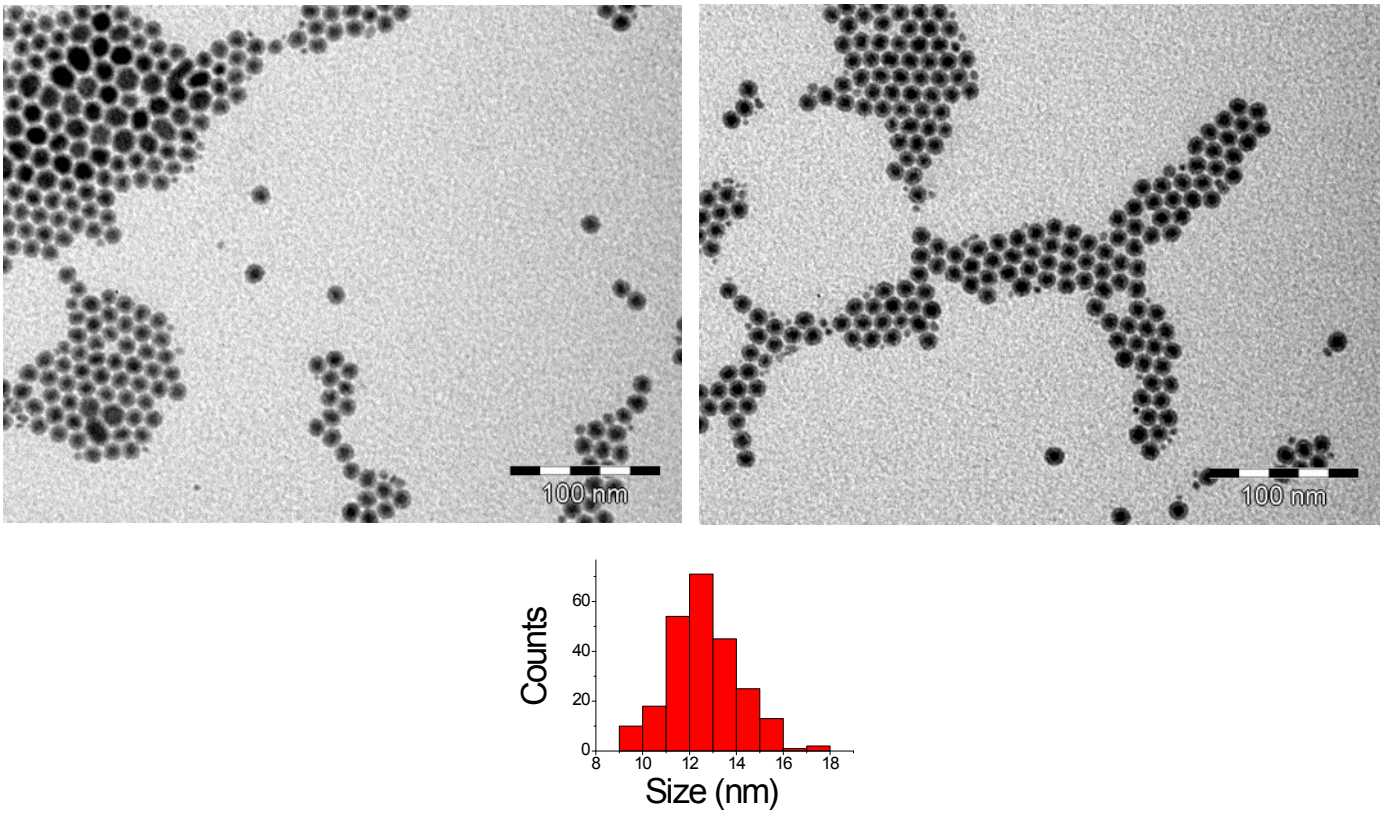

Figure S26. TEM images and size distribution of NPs **FeC-7** obtained after addition of 100 mg of a 1:1 mixture of PA and HDA.

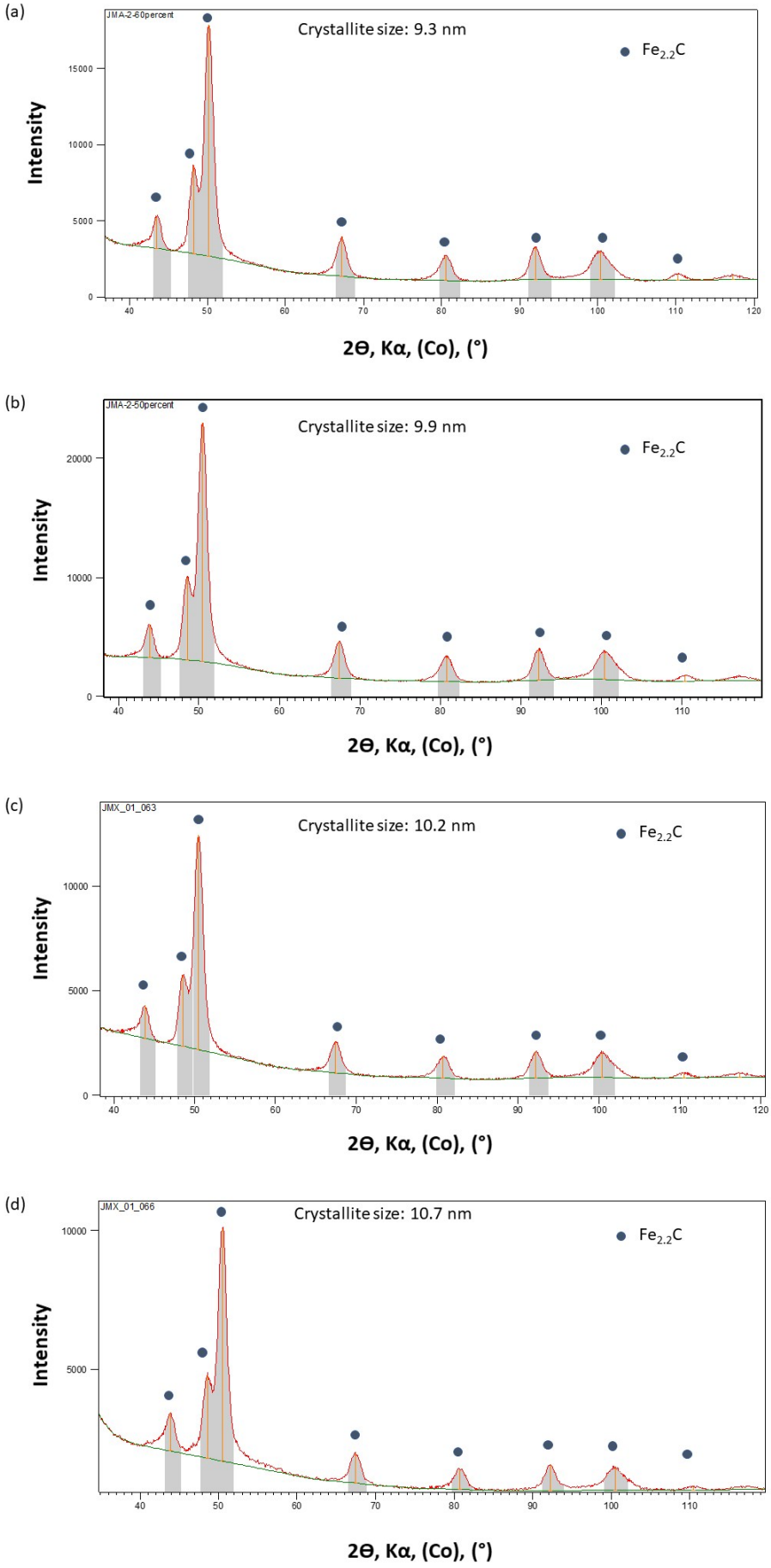

Figure S27. XRD diffractograms of NPs (a) **FeC-4**, (b) **FeC-5**, (c) **FeC-6** and (d) **FeC-7** and crystallite sizes calculated by the Scherrer equation. The labelled peaks correspond to the $Fe_{2.2}C$ phase.

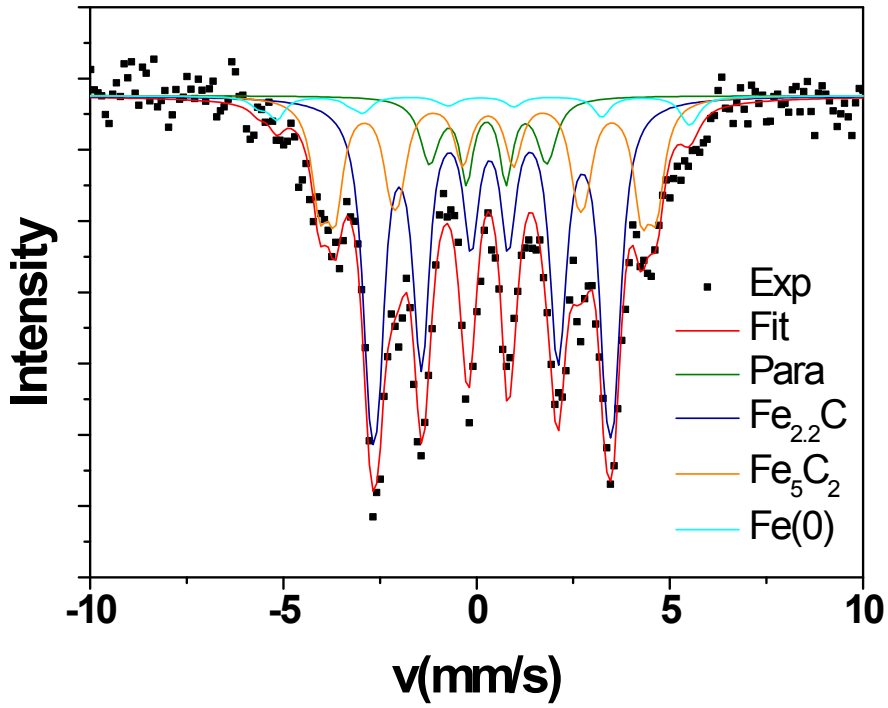

Phases	δ (mm/s)	Q (mm/s)	μ_0H_{hyp} (T)	W (mm/s)	%	
Paramagnetic species	0.25	1.02		0.2	4.9	10.5
	0.30	3.00		0.3	5.6	
$Fe_{2.2}C$	0.36	0.03	18.1	0.2	17.7	55.8
	0.37	0.03	19.5	0.25	38.1	
Fe_5C_2	0.29		27.0	0.25	14.3	29.1
	0.36		24.6	0.25	14.8	
Fe(0)	0		35.0	0.25	1.4	4.6
	0.15		33.0	0.25	3.2	

Figure S28. Low temperature (4 K) Mössbauer study of iron carbide nanoparticles **FeC-5**. (a) Mössbauer spectrum, (b) fitting parameters and resulting nanoparticles composition.

SI.8. Characterization of NPs FeC-8 and FeC-9.

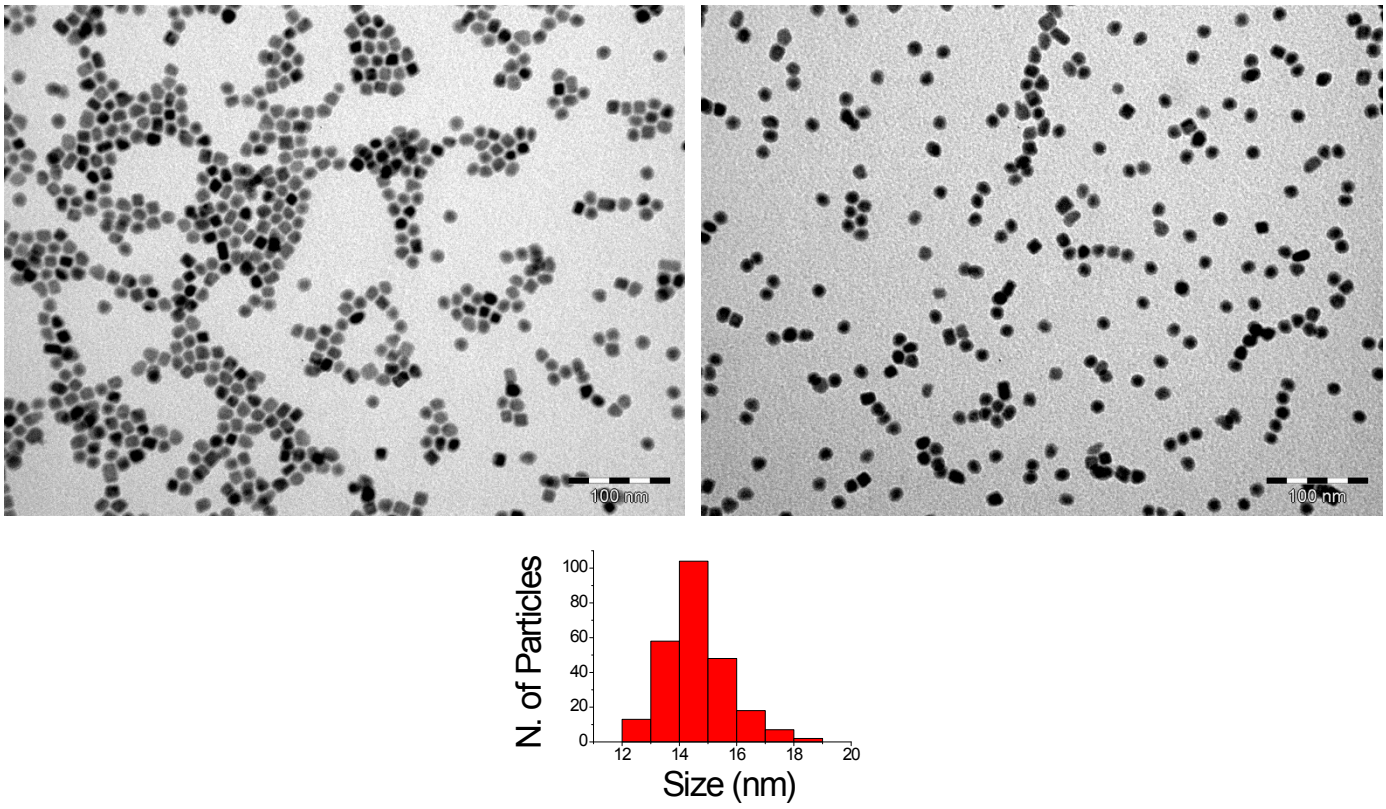

Figure S29. TEM images and size distribution of NPs **FeC-8** obtained after addition of 50 mg of PA.

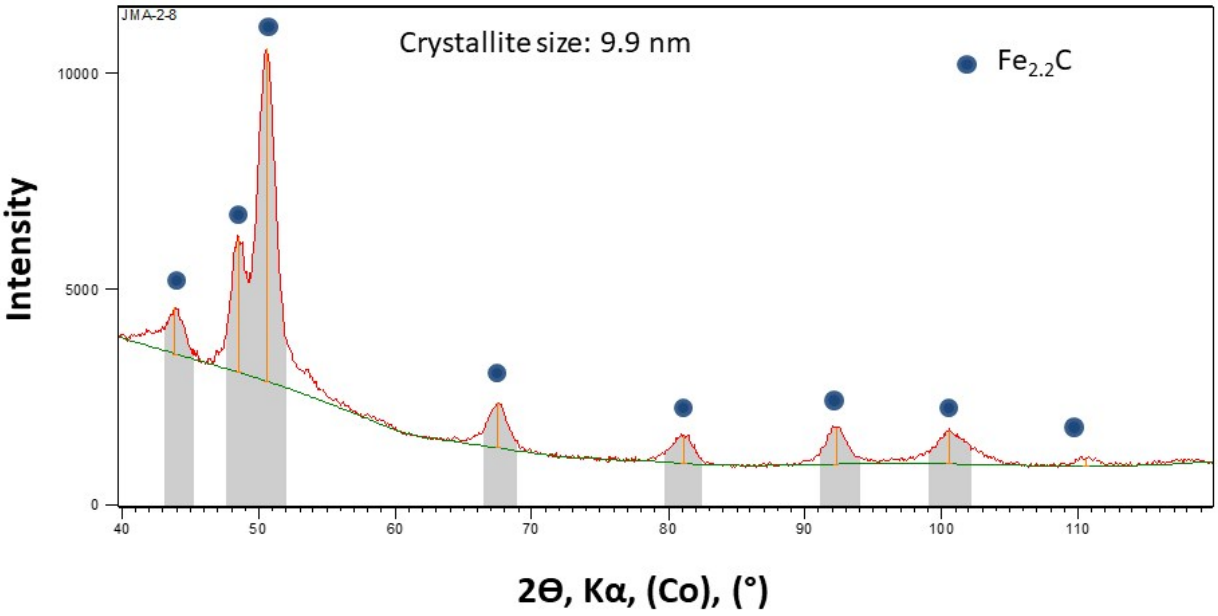

Figure S30. XRD diffractogram of NPs **FeC-8**. The labelled peaks correspond to the $Fe_{2.2}C$ phase.

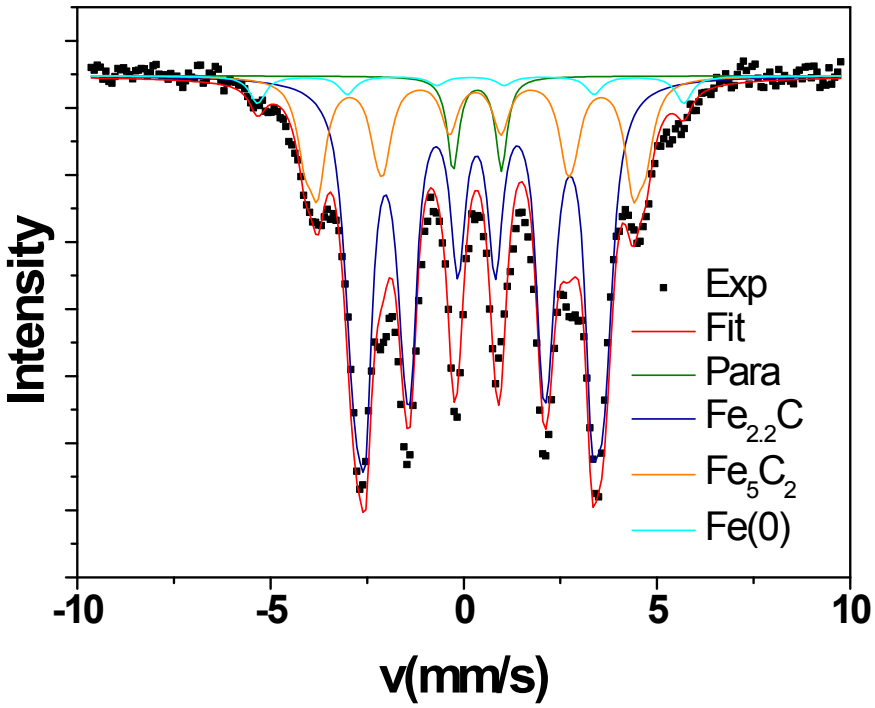

Phases	δ (mm/s)	Q (mm/s)	$\mu_0 H_{hyp}$ (T)	W (mm/s)	%	
Paramagnetic species	0.31	1.02		0.2	4.9	4.1
$Fe_{2.2}C$	0.36	0.03	18.1	0.2	25.1	69.6
	0.37	0.03	19.5	0.25	44.5	
Fe_5C_2	0.29		27.0	0.25	14.4	24.8
	0.36		24.6	0.25	10.4	
Fe(0)	0		35.0	0.25	1.1	1.5
	0.15		33.0	0.25	0.4	

Figure S31. Low temperature (4 K) Mössbauer study of iron carbide nanoparticles **FeC-8**. (a) Mössbauer spectrum, (b) fitting parameters and resulting nanoparticles composition.

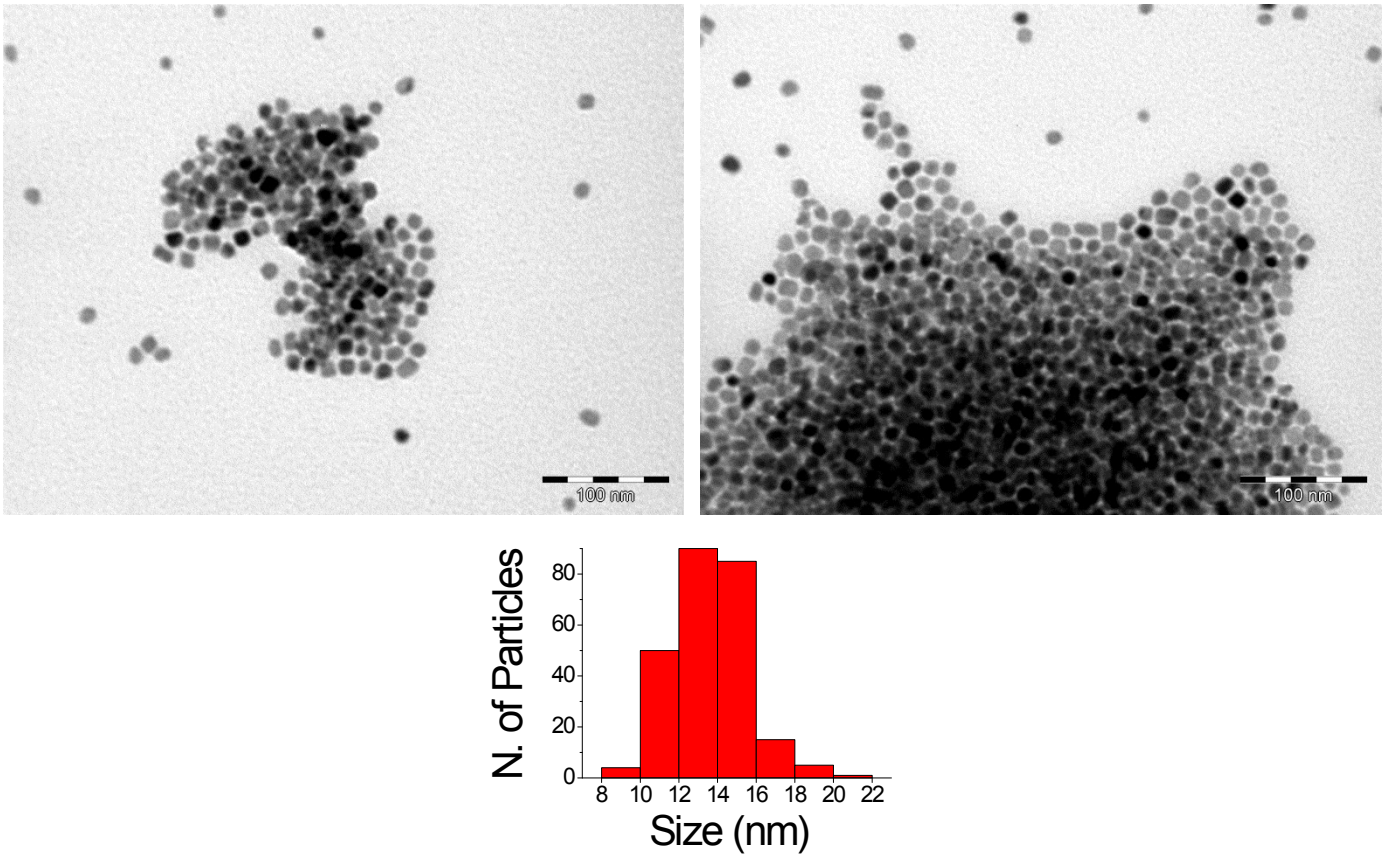

Figure S32. TEM images and size distribution of NPs **FeC-9** obtained after addition of 50 mg of HDA.

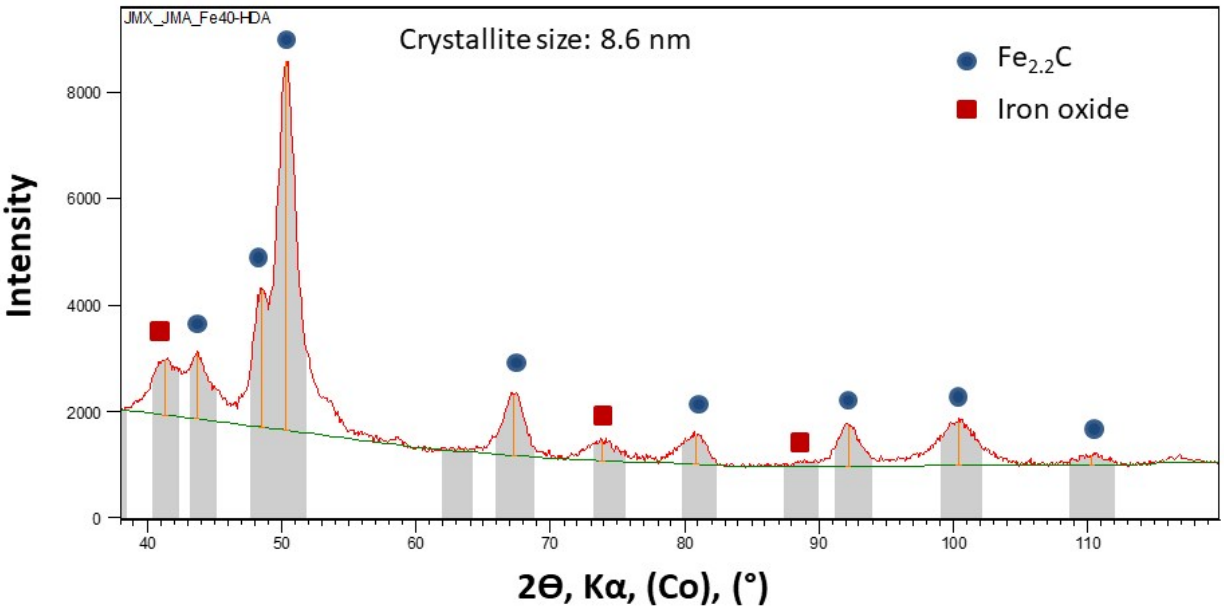

Figure S33. XRD diffractogram of NPs **FeC-9**. The peaks labelled in blue correspond to the $Fe_{2.2}C$ phase and the peaks labelled in red correspond to iron oxide.

SI.9. High-frequency hysteresis loops as a function of time for NPs FeC-5 and FeC-8.

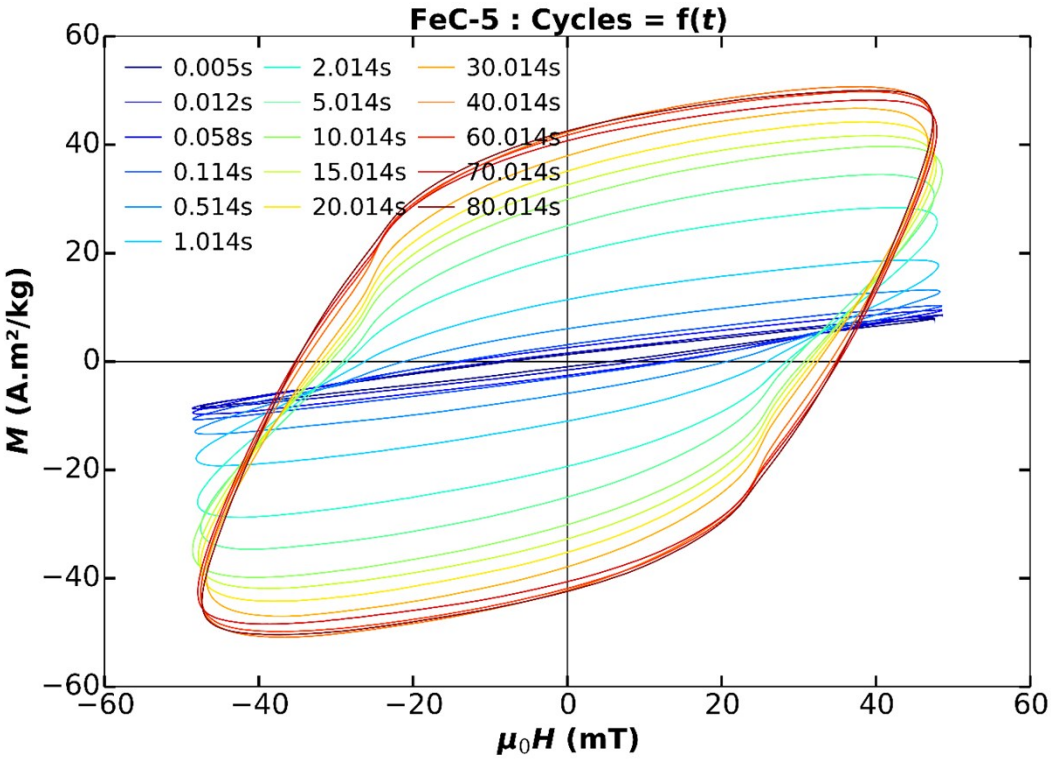

Figure S34. High-frequency hysteresis loops as a function of time for NPs **FeC-5** when applying an alternating magnetic field of $\mu_0 H_{rms}$ of 33 mT with a f of 50 kHz

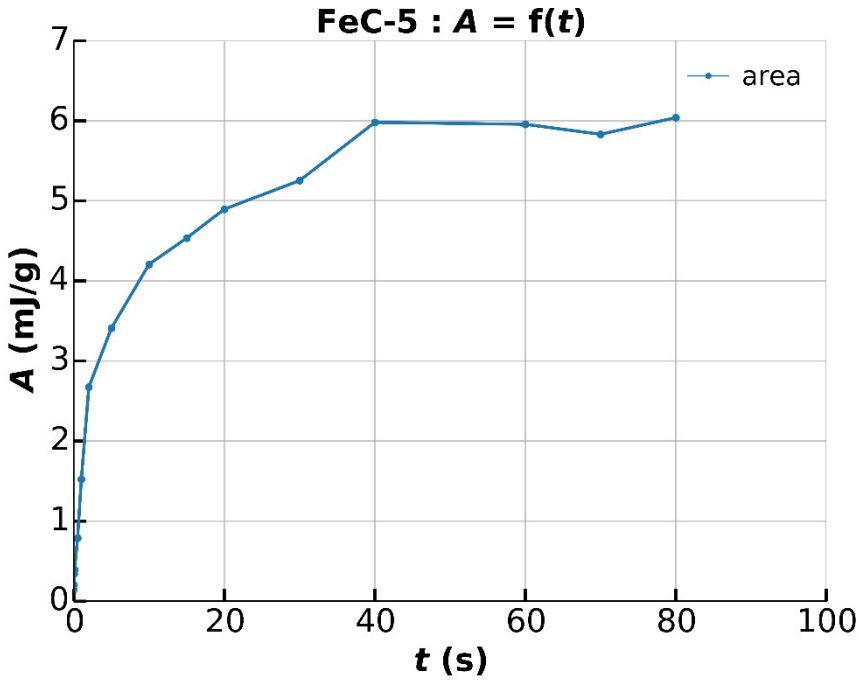

Figure S35. Evolution of the area of the hysteresis cycles as a function of time for NPs **FeC-5** when applying an alternating magnetic field of $\mu_0 H_{rms}$ of 33 mT with a f of 50 kHz.

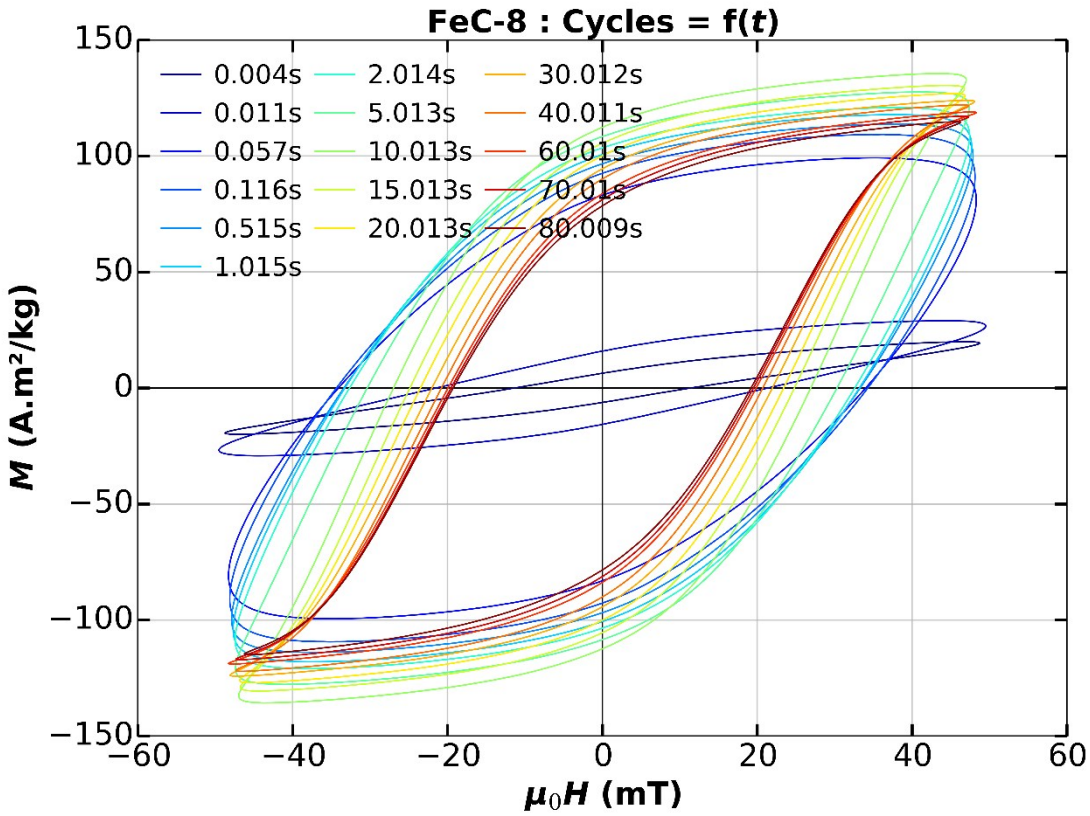

Figure S36. High-frequency hysteresis loops as a function of time for NPs **FeC-8** when applying an alternating magnetic field of $\mu_0 H_{rms}$ of 33 mT with a f of 50 kHz

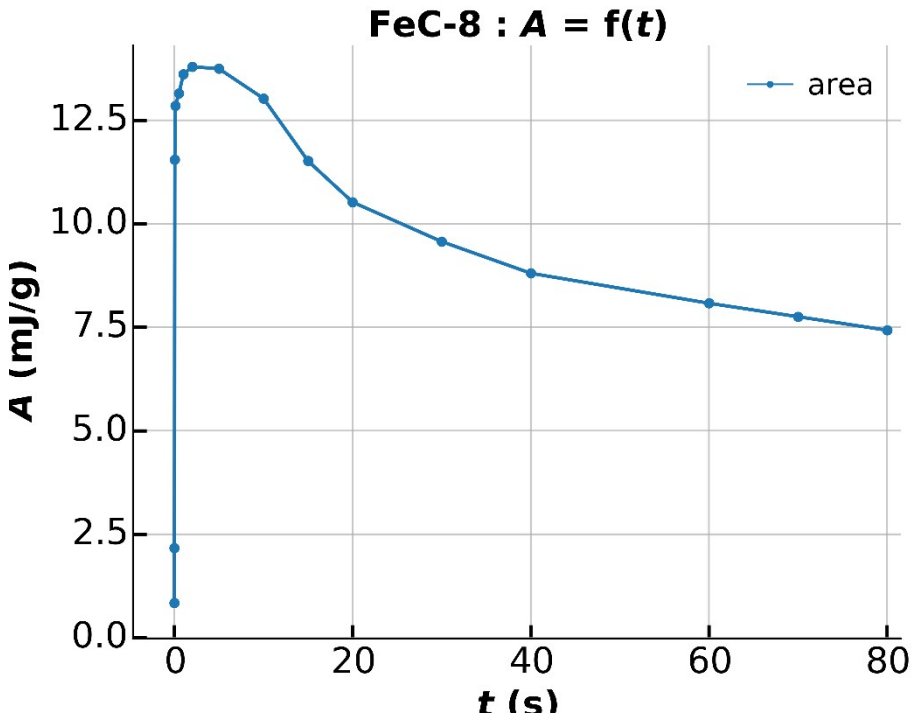

Figure S37. Evolution of the area of the hysteresis cycles as a function of time for NPs **FeC-8** when applying an alternating magnetic field of $\mu_0 H_{rms}$ of 33 mT with a f of 50 kHz.

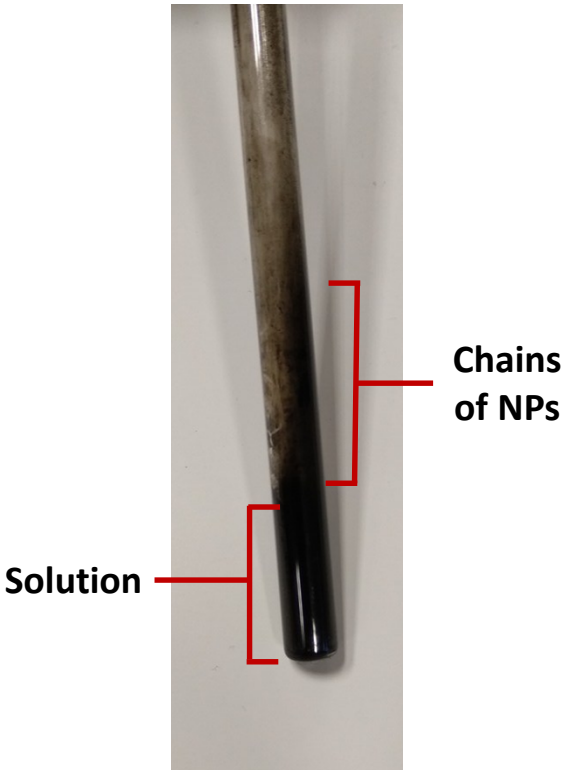

Figure S38. Image of the glass tube after measurement of the high-frequency hysteresis loops of NPs **FeC-8**, showing that the chains of NPs formed during the experiments were coming out from the solution.

SI.10. References

1. A. Bordet, L.-M. Lacroix, P.-F. Fazzini, J. Carrey, K. Soulantica and B. Chaudret, *Angew. Chem., Int. Ed.*, 2016, **55**, 15894-15898.